The Meteoritical Society

Meteoritics & Planetary Science 42, Nr 7/8, 1197–1219 (2007)
Abstract available online at http://meteoritics.org

Remelting of refractory inclusions in the chondrule-forming regions: Evidence from chondrule-bearing type C calcium-aluminum-rich inclusions from Allende

Alexander N. KROT[1], Hisayoshi YURIMOTO[2], Ian D. HUTCHEON[3], Marc CHAUSSIDON[4], Glenn J. MACPHERSON[5], and Julie PAQUE[6]

[1]Hawai‘i Instititute of Geophysics and Planetology, School of Ocean and Earth Science and Technology, University of Hawai‘i at Manoa, Honolulu, Hawai‘i 96822, USA
[2]Department of Earth and Planetary Sciences, Tokyo Institute of Technology, Meguro, Tokyo 152-8551, Japan
[3]Glenn T. Seaborg Institute, Lawrence Livermore National Laboratory, Livermore, California 94451, USA
[4]CRPG-CNRS, BP 20, 15 rue Notre Dame des Pauvres, 54501 Vandoeuvre-lès-Nancy Cedex, France
[5]Smithsonian Institution, Department of Mineral Sciences, NHB 119, Washington, D.C. 20560, USA
[6]Division of Geological and Planetary Sciences, California Institute of Technology, Pasadena, California 91125, USA
*Corresponding author. E-mail: sasha@higp.hawaii.edu

(Received 02 June 2006; revision accepted 08 June 2007)

The appendix for this article is available online at http://meteoritics.org.

Abstract–We describe the mineralogy, petrology, oxygen, and magnesium isotope compositions of three coarse-grained, igneous, anorthite-rich (type C) Ca-Al-rich inclusions (CAIs) (ABC, TS26, and 93) that are associated with ferromagnesian chondrule-like silicate materials from the CV carbonaceous chondrite Allende. The CAIs consist of lath-shaped anorthite (An_{99}), Cr-bearing Al-Ti-diopside (Al and Ti contents are highly variable), spinel, and highly åkermanitic and Na-rich melilite ($Åk_{63–74}$, 0.4–0.6 wt% Na_2O). TS26 and 93 lack Wark-Lovering rim layers; ABC is a CAI fragment missing the outermost part. The peripheral portions of TS26 and ABC are enriched in SiO_2 and depleted in TiO_2 and Al_2O_3 compared to their cores and contain relict ferromagnesian chondrule fragments composed of forsteritic olivine ($Fa_{6–8}$) and low-Ca pyroxene/pigeonite ($Fs_1Wo_{1–9}$). The relict grains are corroded by Al-Ti-diopside of the host CAIs and surrounded by haloes of augite ($Fs_{0.5}Wo_{30–42}$). The outer portion of CAI 93 enriched in spinel is overgrown by coarse-grained pigeonite ($Fs_{0.5–2}Wo_{5–17}$), augite ($Fs_{0.5}Wo_{38–42}$), and anorthitic plagioclase (An_{84}). Relict olivine and low-Ca pyroxene/pigeonite in ABC and TS26, and the pigeonite-augite rim around 93 are ^{16}O-poor ($\Delta^{17}O$ ~ –1‰ to –8‰). Spinel and Al-Ti-diopside in cores of CAIs ABC, TS26, and 93 are ^{16}O-enriched ($\Delta^{17}O$ down to −20‰), whereas Al-Ti-diopside in the outer zones, as well as melilite and anorthite, are ^{16}O-depleted to various degrees ($\Delta^{17}O$ = –11‰ to 2‰). In contrast to typical Allende CAIs that have the canonical initial $^{26}Al/^{27}Al$ ratio of ~5 × $10^{–5}$, ABC, 93, and TS26 are ^{26}Al-poor with $(^{26}Al/^{27}Al)_0$ ratios of (4.7 ± 1.4) × $10^{–6}$, (1.5 ± 1.8) × $10^{–6}$, and <1.2 × $10^{–6}$, respectively. We conclude that ABC, TS26, and 93 experienced remelting with addition of ferromagnesian chondrule silicates and incomplete oxygen isotopic exchange in an ^{16}O-poor gaseous reservoir, probably in the chondrule-forming region. This melting episode could have reset the ^{26}Al-^{26}Mg systematics of the host CAIs, suggesting it occurred ~2 Myr after formation of most CAIs. These observations and the common presence of relict CAIs inside chondrules suggest that CAIs predated formation of chondrules.

INTRODUCTION

Chondrules and refractory inclusions (Ca-Al-rich inclusions [CAIs] and amoeboid olivine aggregates [AOAs]) are the major high-temperature components of chondritic meteorites that can potentially allow dating of the earliest processes in the solar nebula (e.g., Amelin et al. 2002; Kita et al. 2005). Mineralogical, chemical, and isotopic data suggest that CAIs and AOAs formed in an ^{16}O-rich gaseous reservoir [$\Delta^{17}O_{SMOW}$ ~ –20‰, where $\Delta^{17}O = \delta^{17}O - 0.52 \times \delta^{18}O$, $\delta^{17,18}O = [(^{17,18}O/^{16}O)_{sample}/(^{17,18}O/^{16}O)_{SMOW} - 1] \times 1000$; SMOW is standard mean ocean water] at high ambient temperatures (near or above the condensation temperature of forsterite ~1375 K at a total pressure of 10^{-4} bar), and were subsequently isolated (physically or kinetically) from reactions with the high-temperature solar nebula gas (e.g., Krot et al. 2001a, 2002a, 2002b, 2004a, 2004b, 2005a; MacPherson 2003; Scott and Krot 2003). Evaporation and condensation are believed to have been the dominant processes during the formation of refractory inclusions (e.g., Grossman et al. 2002; Richter et al. 2002; MacPherson 2003). Subsequently, some CAIs experienced extensive melting accompanied by evaporation and mass-dependent isotopic fractionation of magnesium and possibly silicon (Grossman et al. 2002; Richter et al. 2002; Davis et al. 2005). Both igneous and nonigneous CAIs are surrounded by multilayered Wark-Lovering rims, with the outermost layers, which were composed of Al-diopside and forsterite, probably formed by condensation (Wark and Lovering 1977; Wark and Boynton 2001). Contrary to refractory inclusions, most chondrules originated in an ^{16}O-poor (Δ^{17}O > –5‰) gaseous reservoir (Krot et al. 2005a, 2006a) at low (<1000 K) ambient temperatures and high total pressure or dust/gas ratios (Galy et al. 2000; Alexander and Wang 2001; Desch and Connolly 2002). Melting of pre-existing solids accompanied by evaporation-recondensation is believed to have been the dominant process during chondrule formation (e.g., Jones et al. 2000; Desch and Connolly 2002; Cuzzi and Alexander 2006).

One of the major questions in cosmochemistry concerning the origin of CAIs and chondrules is their relative chronology (Alexander 2003; Kita et al. 2005). This relative chronology can be potentially resolved using the short-lived radionuclide ^{26}Al, which decays to ^{26}Mg with a half-life of 0.73 Myr and which was present in the nebula regions where CAIs and chondrules formed (e.g., MacPherson et al. 1995; Russell et al. 1996; Kita et al. 2000; Huss et al. 2001; Mostefaoui et al. 2002; Bizzarro et al. 2004). Most CAIs show large ^{26}Mg excesses (^{26}Mg*) corresponding to a "canonical" initial ^{26}Al/^{27}Al ratio [(^{26}Al/^{27}Al)$_0$] of ~5×10^{-5} (MacPherson et al. 1995), whereas most chondrules have significantly smaller ^{26}Mg*, corresponding to (^{26}Al/^{27}Al)$_0$ of <1.2×10^{-5} (e.g., Kita et al. 2000; Huss et al. 2001; Mostefaoui et al. 2002; Kita et al. 2005 and references therein). Based on these observations and the assumption that ^{26}Al was uniformly distributed in the solar nebula,[1] it is generally inferred that CAIs formed at least 1–1.5 Myr before chondrules (MacPherson et al. 1995; Russell et al. 1996; Kita et al. 2000; Huss et al. 2001; Mostefaoui et al. 2002). This conclusion has recently been questioned based on the lead (Amelin et al. 2002, 2004) and magnesium isotope measurements of CV chondrules and CAIs (Bizzarro et al. 2004). The ^{207}Pb-^{206}Pb ages of the Allende chondrules (4566.7 ± 1.0 Ma) (Amelin et al. 2004) cannot be distinguished from those of the CV CAIs (4567.2 ± 0.6 Ma) (Amelin et al. 2002). Bizzarro et al. (2004) reported a range of (^{26}Al/^{27}Al)$_0$ from (5.66 ± 0.80) to (1.36 ± 0.52) × 10^{-5} in Allende chondrules and concluded that chondrule formation began contemporaneously with the formation of CAIs, and continued for at least 1.4 Myr.

[1]Based on the precise bulk Mg isotope measurements of different chondrite groups and samples from the Moon, Mars, and aether, Thrane et al. (2006) concluded that ^{26}Al was uniformly distributed in the inner solar system.

We note, however, that the (^{26}Al/^{27}Al)$_0$ ratios inferred from the magnesium isotope measurements of whole chondrules (Bizzarro et al. 2004) may date the time for the formation of chondrule precursor materials, not the time of chondrule melting; establishing the latter requires magnesium isotope measurements of mineral separates or individual mineral grains, which has not been done yet. In addition, spatial heterogeneity in ^{26}Al distribution in the solar nebula cannot be ruled out (e.g., Gounelle et al. 2001, 2006). On the other hand, the relative chronology of CAI and chondrule formation can be resolved by studying compound objects composed of chondrule and CAI, because both constituents of such objects must have been affected by the same heating episode. All CAI-chondrule compound objects consist of relict CAIs inside chondrules, suggesting that the host chondrules formed by melting of solid precursors containing CAIs formed earlier (Misawa and Nakamura 1988; Maruyama et al. 1999; Krot and Keil 2002; Krot et al. 1999, 2001b, 2002c, and 2004c; Maruyama and Yurimoto 2003; Russell et al. 2005). The only exception is the chondrule-bearing CAI A5 from the Yamato-81020 chondrite that was interpreted as an evidence for chondrule formation predating formation of CAIs by Itoh and Yurimoto (2003).

Here, we report the mineralogy, petrography, and oxygen and magnesium isotope compositions of three coarse-grained, igneous CAIs from Allende (ABC, TS26, and 93) that are closely associated with ferromagnesian chondrule-like silicate materials from Allende. Our results provide important constraints on the relative chronology of CAI and chondrule formation. The mineralogy and petrology of ABC and TS26 have been previously characterized (Grossman 1973; Macdougall et al. 1981; Wark 1987); however, the presence of relict chondrule material inside them remained unnoticed. Preliminary results with isotope data for ABC and TS26, has recently been published (Krot et al. 2005b).

SAMPLES AND ANALYTICAL PROCEDURES

All sections were carbon-coated; ABC and TS26 had been previously gold-coated. Because the sections were either very thin or partly detached from the glass slides, we decided to use the old carbon coating. As a result, some of the opaque nodules in TS26 were identified only tentatively as Fe,Ni metal or Fe,Ni-sulfides.

The CAIs were studied using optical microscopy (in transmitted light only), backscattered electron (BSE) imaging, X-ray elemental mapping, and electron probe

Table 1.[a] Representative compositions of plagioclase in the Allende type C CAIs ABC, TS26, and 93.

CAI	ABC	ABC	TS26	TS26	TS26	93	93	93	93
Ox/an. no.	1	2	3	4	5	6	7	8	9
SiO_2	41.9	45.6	42.0	42.3	43.5	42.1	42.8	46.0	46.4
TiO_2	0.09	0.09	<0.03	<0.03	0.03	0.09	<0.03	<0.03	<0.03
Al_2O_3	37.3	33.4	36.7	36.4	36.0	37.1	37.0	33.5	33.5
Cr_2O_3	<0.06	<0.06	<0.06	<0.06	<0.06	<0.06	<0.06	<0.06	<0.06
FeO	0.07	1.5	0.35	0.40	0.21	0.18	0.14	0.86	0.21
MnO	<0.06	<0.06	0.07	<0.06	<0.06	<0.06	0.05	<0.06	<0.06
MgO	0.05	0.41	0.04	0.05	0.05	0.03	0.04	0.43	0.67
CaO	20.3	17.2	19.9	19.7	18.4	20.3	20.1	17.6	18.1
Na_2O	<0.06	1.9	0.10	0.23	0.78	0.10	0.07	1.7	1.3
K_2O	<0.06	<0.06	<0.06	<0.06	<0.06	<0.06	<0.06	<0.06	<0.06
Total	99.6	100.1	99.2	99.0	99.0	99.9	100.2	100.1	100.2
An, mol%	99.0	83.0	99.1	97.9	92.9	99.1	99.4	85.1	88.8

[a]Abbreviations: an. no. = analysis number; ox = oxide. 1 = CAI core and mantle; 2 = near relict olivine-pyroxene fragment (see Fig. 2f); 3 = CAI core; 4 = CAI mantle; 6 = coarse-grained, lath-shaped in the CAI core; 7 = fine-grained, interstitial in the CAI core (see Fig. 10f); 8 = in the coarse-grained pigeonite-augite-rich region (see Fig. 10a); 9 = in the fine-grained augite-rich region (see Fig. 10g).

microanalysis (EPMA). X-ray elemental maps with a resolution of 2–5 μm/pixel were acquired with five spectrometers of a Cameca microprobe operating at a 15 kV accelerating voltage, 50–100 nA beam currents, and a beam size of ~1–2 μm. BSE images were obtained with a JEOL JSM-5900LV scanning electron microscope (SEM) using a 15 kV accelerating voltage and a 1–2 nA beam current. Wavelength dispersive X-ray spectroscopy (WDS) microanalyses were performed with a Cameca SX-50 electron microprobe at the University of Hawai‘i using a 15 kV accelerating voltage, a 10 nA beam current, and a beam size of ~1–2 μm. For each element, the counting time on both peak and background was 20 s (10 s for Na and K). Matrix corrections were applied using a PAP software routine. The detection limits (in wt%) of the Cameca SX-50 for silicates and oxides are 0.03 (SiO_2, TiO_2, Al_2O_3, MgO), 0.04 (CaO), 0.06 (Na_2O, K_2O, Cr_2O_3, MnO), and 0.07 (FeO).

In situ oxygen isotope analyses of ABC and TS26 were carried out using a modified Cameca 1270 ion microprobe at the Tokyo Institute of Technology. A primary ion beam of Cs^+ with 20 keV impact energy was used to excavate shallow pits of ~3 × 5 μm across. The primary beam current was adjusted for each measurement to obtain a count rate of $^{16}O^-$ ions of ~3.5 to 4 × 10^5 cps. Each measurement consisted of 60 cycles of 40 s each and about 10–20 min presputtering to remove the carbon coating. A normal-incident electron gun was used for charge compensation of analyzed areas. Negative secondary ions from the ^{16}O tail, ^{16}O, ^{17}O, ^{16}OH, and ^{18}O were analyzed at a mass-resolving power of ~6000, sufficient to completely separate ^{16}OH interference on ^{17}O. Secondary ions were detected by an electron multiplier (EM) in pulse-counting mode, and analyses were corrected for EM dead time. Instrumental mass fractionation (IMF) was corrected using San Carlos olivine as a standard. The precision of individual measurements (1σ) is ~1.7‰ for $\delta^{18}O$ and ~2.5‰ for $\delta^{17}O$.

Oxygen isotope compositions of CAI 93 were measured with the CRPG-CNRS Cameca IMS 1270 ion microprobe operated in multicollection mode. All three oxygen isotopes were measured simultaneously using Faraday cups (FCs): ^{16}O and ^{18}O were measured using multicollector FCs while ^{17}O was measured using the monocollector FC. A Cs^+ primary beam of 10 nA was used to produce ellipsoid sputter pits approximately 25–30 μm in size. The IMF for $^{18}O/^{16}O$ ratio was calculated using terrestrial diopside as a standard. Since the monocollector FC is not intercalibrated with the multicollector FCs, the yield of the former was calculated to have the standard on the terrestrial fractionation line of slope 0.52. Corrections for IMF, counting statistics, and uncertainty in the standard composition were applied. The precision (2σ) of individual analyses is better than 1‰ for both $\delta^{18}O$ and $\delta^{17}O$. Before and after oxygen isotope measurements, the CAIs were examined in BSE and SE images to verify the locations of the sputtered craters and the mineralogy of the phases analyzed.

Magnesium isotope compositions of ABC, TS26, and CAI 93 were measured using the Panurge, a modified Cameca IMS-3f ion microprobe at LLNL using the operating conditions and procedures described in Kennedy et al. (1992). The Mg isotope ratios were corrected for both instrumental and intrinsic fractionation assuming the standard ratios of $^{25}Mg/^{24}Mg = 0.12663$ and $^{26}Mg/^{24}Mg = 0.13932$ (Catanzaro et al. 1966). The corrected ratios $(^{26}Mg/^{24}Mg)_C$ were used to calculate the excess of ^{26}Mg ($\delta^{26}Mg^*$): $\delta^{26}Mg^* = [(^{26}Mg/^{24}Mg)_C/0.13932 - 1] \times 1000$.

RESULTS

Mineralogy and Petrography

ABC is a coarse-grained, igneous, anorthite-rich (type C) CAI fragment composed of lath-shaped anorthite (An_{99})

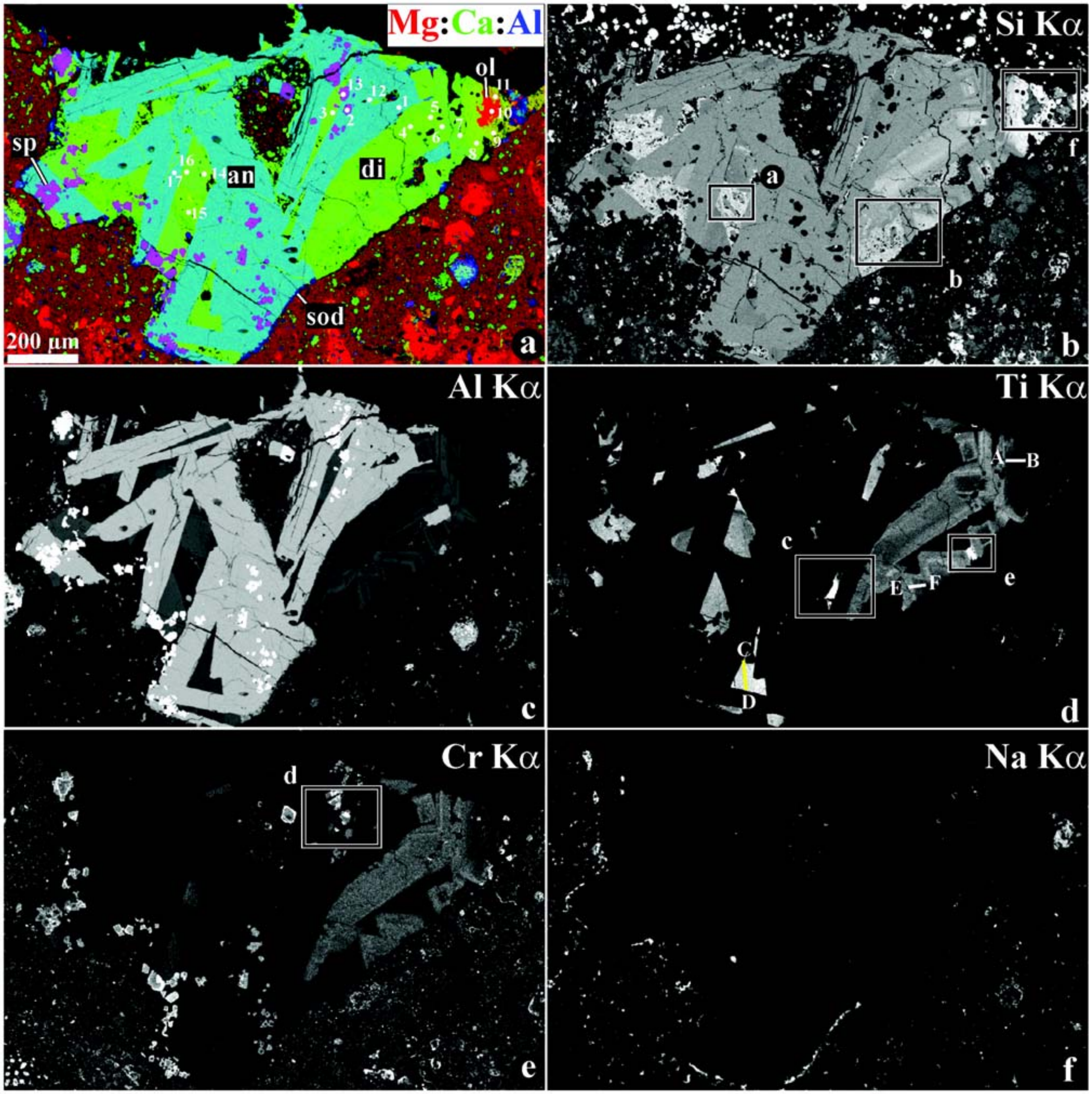

Fig. 1. a) Combined elemental map in Mg (red), Ca (green), and Al Kα (blue) X-rays and b) elemental maps in Si, c) Al, d) Ti, e) Cr, and f) Na Kα of a type C CAI fragment ABC from Allende. Regions outlined and labelled from (a) to (f) are shown in detail in Figs. 2a–f, respectively. Numbered white dots in (a) correspond ion probe spots of oxygen isotope analyses listed in Table 7. The CAI consists of coarse-grained, anorthite laths and Al-Ti-diopside, both poikilitically enclosing spinel grains, and fine-grained interstitial material rich in Si. Anorthite is slightly replaced by sodalite. Relict olivine-pigeonite fragment occurs in the right portion of the CAI. The Al-Ti-diopside grains in this portion show complex oscillatory zoning and are enriched in Cr relative to those in the left portion of the CAI. AB, CD, and EF indicate compositional profiles shown in Fig. 4. an = anorthite; di = Al-Ti-diopside; ol = olivine; sod = sodalite; sp = spinel.

(Table 1) and Al-Ti-diopside, both poikilitically enclosing spinel grains, and fine-grained, porous interstitial material (Figs. 1 and 2). The Al-Ti-diopside grains show significant compositional variations that are linked to their position in the CAI. Grains in the left portion of the fragment (shown in Fig. 1; labeled as “core” in Fig. 3) are enriched in TiO_2 and Al_2O_3 and depleted in Cr_2O_3 compared to those in the right portion (labeled as “mantle” in Fig. 3): 5.6 ± 1.2 versus 3.4 ± 0.8; 16.9 ± 2.0 versus 13.1 ± 2.9; 0.35 ± 0.25 versus 1.2 ± 0.2, respectively (Table 2; Fig. 3). The Al-Ti-diopside grains in the mantle show complex oscillatory zoning with the edges enriched in Al_2O_3 and TiO_2 and depleted in MgO and SiO_2

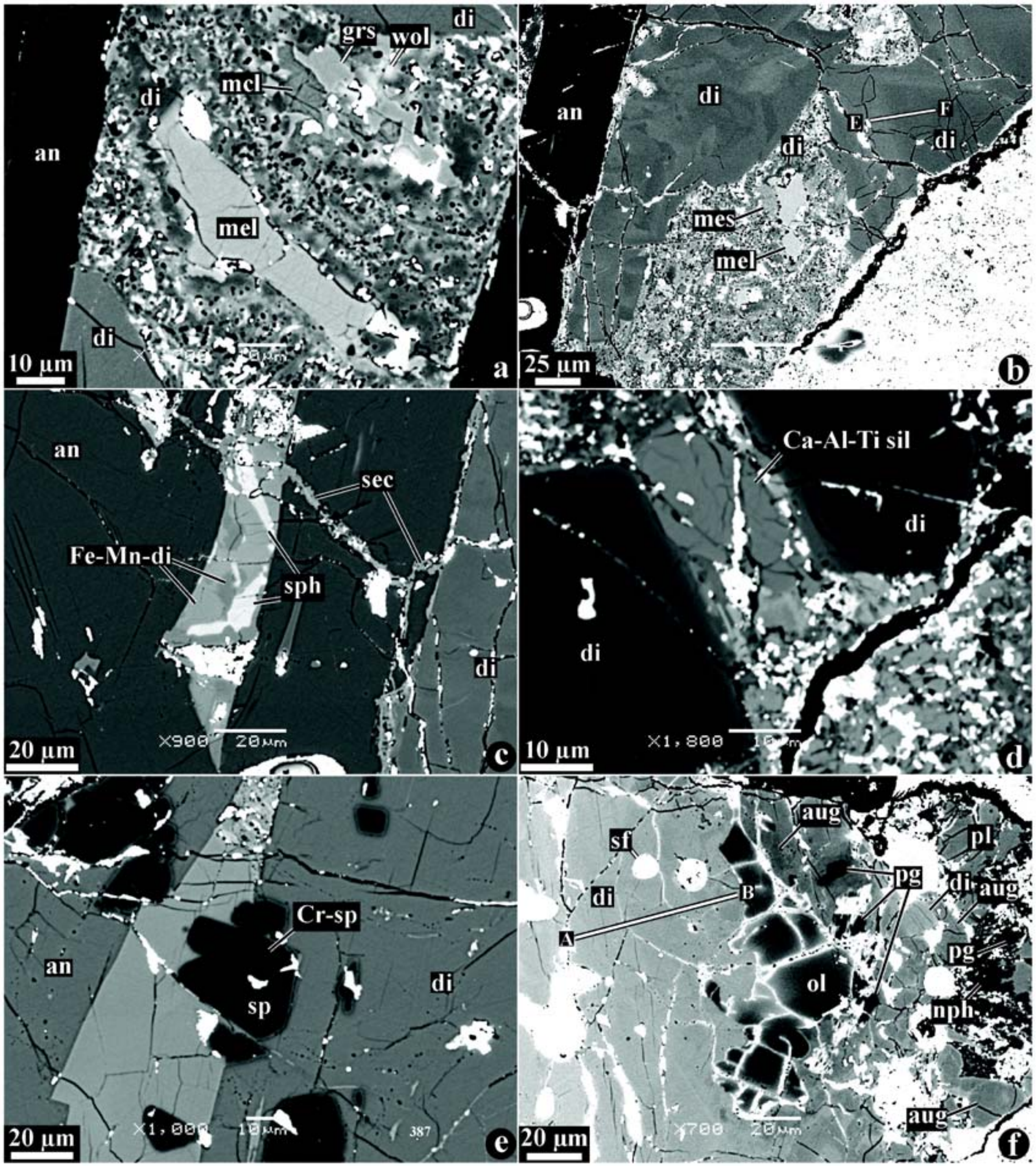

Fig. 2. BSE images of the Allende CAI ABC. a–d) Interstitial regions between coarse anorthite and Al-Ti-diopside grains. Bright white grains are gold left after coating. EF and AB in (f) and (b) indicate compositional profiles shown in Fig. 4. a) and b) The interstitial regions are porous and composed of melilite, fine-grained Al-diopside, grossular, monticellite, wollastonite, and very fine-grained mesostasis. c) Iron-manganese-bearing Al-diopside and sphene. d) Unidentified Ca-Al-Ti-silicate. e) Euhedral spinel grains poikilitically enclosed by anorthite and Al-Ti-diopside show enrichment in chromium. f) Relict polymineral mineral fragment composed of forsterictic olivine, pigeonite, Al-Ti–poor diopside, and anorthitic plagioclase. The fragment is surrounded by a halo of augite. Abbreviations: an = anorthite; aug = augite; Ca-Al-Ti sil = unidentified Ca-Al-Ti-silicate; Cr-sp = chromium-bearing spinel; di = Al-Ti-diopside; Fe-Mn-di = Fe- and Mn-bearing Al-Ti-diopside; grs = grossular; mcl = monticellite; mes = very fine-grained mesostasis; nph = nepheline; ol = olivine; pg = pigeonite; pl = anorthitic plagioclase; sec = vein of unidentified secondary minerals; sf = sulfide; sp = spinel; sph = sphene; wol = wollastonite.

compared to their cores (Fig. 4a; Table A1 [available online at http://meteoritics.org]). The Al-Ti-diopside grains in the core show smaller compositional variations (Fig. 4b; Table A1). The fine-grained interstitial material consists of highly åkermanitic and Na-rich melilite ($Åk_{69–74}$; Na_2O ~ 0.5 wt%) (Table 3), Cr-free and Ti-poor Al-diopside (<0.14 wt% TiO_2; 1.5–11.5 wt% Al_2O_3) (Table 2), grossular, wollastonite, monticellite, and very fine-grained "mesostasis" (Figs. 2a and 2b; Table 4). Occasionally, interstitial spaces are occupied by Fe-Mn–bearing (1.8–2.1 wt% MnO; 1.5–4.5 wt% FeO) diopside (Table 2, an. nos. 5 and 6; Fig. 2c), sphene ($CaTiSiO_5$), and an unidentified Ca-Al-Ti-silicate (Table 4). A Ca-Al-Ti-silicate of similar composition $[Ca_3Ti(Al,Ti)_2(Si,Al)_3O_{14}]$ has been previously described in

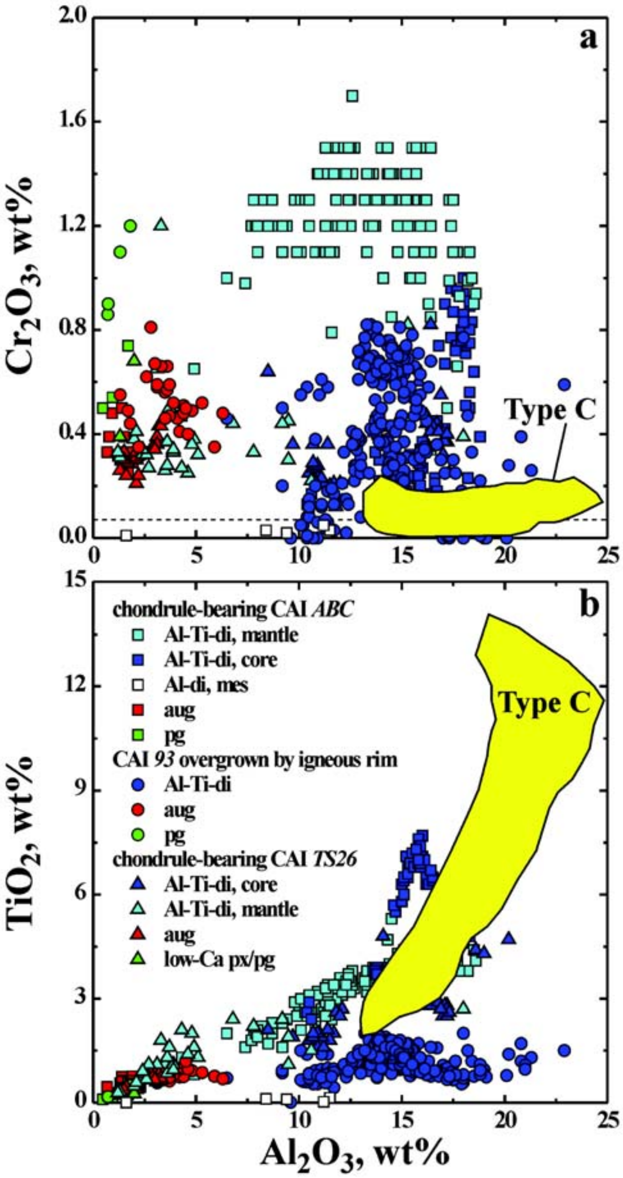

Fig. 3. a) Cr_2O_3 versus Al_2O_3 and b) TiO_2 versus Al_2O_3 (in wt%) in pyroxenes of the chondrule-bearing type C CAIs ABC and TS26, and type C CAI 93 overgrown by a coarse-grained igneous rim from Allende. Yellow regions indicate compositions of pyroxenes in other type C CAIs from Allende (Krot et al. 2007). aug = augite; di = diopside; pg = pigeonite.

several coarse-grained CAIs from Allende and temporarily termed "UNK" (Paque et al. 1994). Sphene is a rare mineral in CAIs; it has been previously described in an extensively altered fine-grained CAI from Allende (McGuire and Hashimoto 1989). The association of Fe-Mn–bearing diopside with sphene and other secondary phases (Fig. 2c) may indicate that this diopside is a secondary mineral. Anorthite around the periphery[2] of the CAI is slightly corroded by sodalite and nepheline (Figs. 1a and 1f). Spinel grains are enriched in Cr along the edges and grain boundaries (Figs. 1e and 2e; Table 5).

A coarse fragment of forsteritic olivine ($Fa_{6–8}$) (Table 6) intergrown with pigeonite ($Fs_1Wo_{7–9}$) (Table 2, an. nos. 7 and 8) occurs in the CAI mantle (Figs. 1 and 2f). Olivine is enriched in FeO (based on the brightness of BSE images) along the cracks. The olivine-pyroxene fragment is corroded by Al-diopside and surrounded by a halo of augite ($Fs_{0.2–0.6}Wo_{30–40}$; 0.18–0.64 wt% TiO_2; 0.77–1.9 wt% Al_2O_3) (Fig. 2f; Tables 2, an. nos. 9 and 10) with rare inclusions of Al,Ti-poor (0.45 wt% TiO_2; 0.67 wt% Al_2O_3) diopside (Table 2, an. no. 11). The Al-Ti-diopside grain in contact with olivine shows oscillatory zoning (Fig. 3c; Table A1). Plagioclase near the olivine-pigeonite fragment is more albitic than in the core (An_{83}) (Table 1) and is replaced by nepheline.

TS26 is an irregularly shaped type C CAI that shows a well-defined core-mantle structure (Fig. 5). A coarse-grained core consists of lath-shaped anorthite (An_{99}) (Table 1) and Al-Ti-diopside, both poikilitically enclosing spinel grains, and interstitial material. The interstitial material is composed of highly åkermanitic and Na-rich melilite ($Åk_{72}$; Na_2O, 0.4 wt%) (Table 3), Al-Ti-diopside, and secondary grossular, monticellite, wollastonite, sodalite, and ferrous olivine (Fig. 6; Table 4). Grossular, monticellite, and wollastonite replace melilite and anorthite (?); sodalite and ferrous olivine replace the interstitial material. Most Al-Ti-diopside grains in the core are sector-zoned and euhedral (Figs. 7a–d, 8a; Table A2); rare fine-grained, anhedral Al-Ti-diopsides are found inside anorthite, which appears to corrode these grains (Figs. 7d–f). The mantle is finer-grained and enriched in Si compared to the core; it is separated from the core by a discontinuous layer of Fe,Ni-sulfides (Figs. 5, 7, and A1 [available online at http://meteoritics.org]) and composed of Al-Ti-diopside, lath-shaped anorthite (An_{98}) (Table 1), and abundant coarse grains of forsteritic olivine ($Fa_{8–17}$) (Table 6) and low-Ca pyroxene ($Fs_1Wo_{1–4}$) (Table 2; Figs. 5b, 7a, 7g–j, A1). The olivine and low-Ca pyroxene grains are extensively corroded by diopside and surrounded by haloes of augite ($Fs_{0.4–0.6}Wo_{35–42}$) (Table 2; Figs. 7g–j, A1); augite is also present in the outermost portion of the mantle.

Type C CAI 93 (Figs. 9 and 10) consists of coarse-grained, Ti-poor, Al-diopside ($Fs_{0.4 \pm 0.3}Wo_{48.2 \pm 1.0}$; [in wt%] TiO_2, 1.2 ± 0.3; Al_2O_3, 14.6 ± 2.3) (Table 2), lath-shaped anorthite ($An_{98.2 \pm 0.6}$) (Table 1), euhedral Ti-poor and Cr-bearing (0.08–0.49 wt% TiO_2; 1.2 ± 0.6 wt% Cr_2O_3) (Table 5) spinel, and interstitial, fine-grained regions composed of highly åkermanitic and Na-rich melilite ($Åk_{63.7 \pm 2.2}$; 0.62 ± 0.07 wt% Na_2O) (Table 3), Ti-poor Al-diopside, and anorthite (An_{99}) (Table 1). The coarse Al-Ti-diopside grains show complex, oscillatory zoning in SiO_2, TiO_2, Al_2O_3, Cr_2O_3, and

[2]Since ABC is fragmented and has no Wark-Lovering rim layers, a location of its periphery was inferred from the presence of relict olivine and low-Ca pyroxene and the highest concentration of the secondary iron-alkali–rich minerals, which are abundant in outer portions of the Allende CAIs (e.g., McGuire and Hashimoto 1989).

Table 2. Representative and average compositions of low-Ca pyroxene, high-Ca pyroxene, and diopside in the Allende type C CAIs ABC, TS26, and 93.

ABC													
Min	Di,core		Di, mantle		Di	Di	Di	Di	Pg	Pg	Aug	Aug	Di
	n = 137	1σ	n = 153	1σ									
Ox/an. no.	1		2		3	4	5	6	7	8	9	10	11
SiO_2	39.9	1.6	43.6	2.5	52.8	50.3	39.5	40.1	58.1	57.4	56.2	53.7	54.1
TiO_2	5.6	1.2	3.4	0.8	0.09	0.05	10.5	8.5	0.09	0.55	0.18	0.64	0.45
Al_2O_3	16.9	2.0	13.1	2.9	4.5	4.2	9.7	12.4	0.45	1.7	0.77	1.9	0.67
Cr_2O_3	0.35	0.25	1.2	0.2	<0.06	<0.06	0.04	0.14	0.50	0.74	0.39	0.33	0.33
FeO	0.55	0.33	0.36	0.71	0.39	2.0	4.5	1.5	0.90	0.45	0.43	0.29	0.23
MnO	0.16	0.08	0.11	0.05	0.06	0.06	2.1	1.8	0.13	0.21	0.09	0.14	0.11
MgO	11.0	0.8	12.4	1.2	16.8	15.6	9.2	10.8	35.4	34.5	25.3	21.1	18.4
CaO	25.1	0.2	25.3	0.3	26.3	28.3	24.0	24.9	5.0	4.5	17.2	21.4	25.1
Na_2O	<0.06	–	<0.06	–	<0.06	<0.06	<0.06	<0.06	<0.06	<0.06	<0.06	<0.06	<0.06
K_2O	<0.06	–	<0.06	–	<0.06	<0.06	<0.06	<0.06	<0.06	<0.06	<0.06	<0.06	<0.06
Total	99.5	0.9	99.5	0.7	100.9	100.5	99.5	100.1	100.5	100.1	100.6	99.5	99.4
Fs, mol%	1.3	0.8	0.8	1.6	0.6	3.2	10.0	3.4	1.3	0.7	0.6	0.5	0.4
Wo, mol%	50.1	0.5	50.8	0.9	50.2	52.8	53.4	52.9	8.6	6.8	32.1	40.7	49.0

Table 2. *Continued*. Representative and average compositions of low-Ca pyroxene, high-Ca pyroxene, and diopside in the Allende type C CAIs ABC, TS26, and 93.

TS26								
Min	Di,core		Di, mantle		Aug		Lpx	Pg
	n = 39	1σ	n = 29	1σ	n = 21	1σ		
Ox/an. no.	12		13		14		15	16
SiO_2	43.7	2.5	50.0	3.2	53.3	0.7	57.2	57.3
TiO_2	2.6	0.8	1.4	0.7	0.49	0.16	0.25	0.22
Al_2O_3	14.0	3.2	5.4	4.1	2.2	0.6	2.0	1.3
Cr_2O_3	0.33	0.16	0.40	0.20	0.32	0.06	0.68	0.39
FeO	0.29	0.11	0.37	0.21	0.45	0.16	0.59	0.58
MnO	0.07	0.03	0.06	0.04	0.08	0.03	0.15	0.09
MgO	12.8	1.4	16.5	2.1	21.2	1.2	36.9	36.4
CaO	24.9	0.3	24.5	1.0	20.6	1.1	1.8	3.0
Na_2O	<0.06	–	<0.06	–	<0.06	–	<0.06	<0.06
K_2O	<0.06	–	<0.06	–	<0.06	–	<0.06	<0.06
Total	98.8	0.3	98.6	0.4	98.7	0.7	99.5	99.2
Fs, mol%	0.6	0.3	0.6	0.3	0.7	0.2	0.9	0.8
Wo, mol%	48.8	0.7	48.1	2.4	39.3	2.4	3.3	5.5

MgO. The outer portions of these grains are enriched in Al_2O_3 and depleted in MgO, SiO_2, TiO_2, and Cr_2O_3 compared to their cores (Fig. 11; Table A3), suggesting coupled substitutions: $Mg^{2+} + Si^{4+} = 2Al^{3+}$ and $Mg^{2+} + Ti^{4+} = 2Al^{3+}$. The observed depletion in chromium toward the grain peripheries could be due to its preferential partitioning into spinel. In the CAI core, coarse-grained anorthite is largely replaced by nepheline and sodalite; in the CAI periphery, anorthite and/or mesostasis(?) are replaced by sodalite, ferrous olivine ($Fa_{\sim 25}$) (Table 4), and nepheline (Fig. 10c). Spinel grains surrounded by iron-alkali–rich secondary minerals show significant enrichment in FeO (from 0.3 to 17.0 wt%) (Table 5); there is no correlation between this enrichment and Cr_2O_3 contents in spinel grains. The interstitial melilite-anorthite-diopside material is replaced by a fine-grained, porous material largely composed grossular, monticellite, and wollastonite; minor secondary nepheline and sodalite occur as well (Figs. 10d–f). The top-left portion of the CAI, shown in Fig. 9, is intergrown with a coarse-grained igneous region composed of Ti-poor, Cr- and Al-bearing augite ($Fs_{0.4 \pm 0.2}Wo_{40.5 \pm 2.3}$; [in wt%] TiO_2, 0.82 ± 0.19; Al_2O_3, 3.6 ± 0.8; Cr_2O_3, 0.53 ± 0.09) (Table 2) overgrowing Ti-poor, Cr- and Al-bearing pigeonite ($Fs_{1.3 \pm 0.67}Wo_{10.4 \pm 5.4}$; [in wt%] TiO_2, 0.30 ± 0.16; Al_2O_3, 1.1 ± 0.5; Cr_2O_3, 1.0 ± 0.17) (Table 2), and anorthitic plagioclase (An_{84}) (Table 1). Plagioclase and possibly mesostasis(?) are extensively replaced by sodalite and ferrous olivine (Figs. 10b and 10c). This coarse-grained region is separated from the CAI by a spinel-rich layer, which may represent a remnant of a Wark-Lovering rim. Most of the anorthite grains in the CAI appear to grow away from this layer toward the CAI core (Figs. 10a and 10c); some of them,

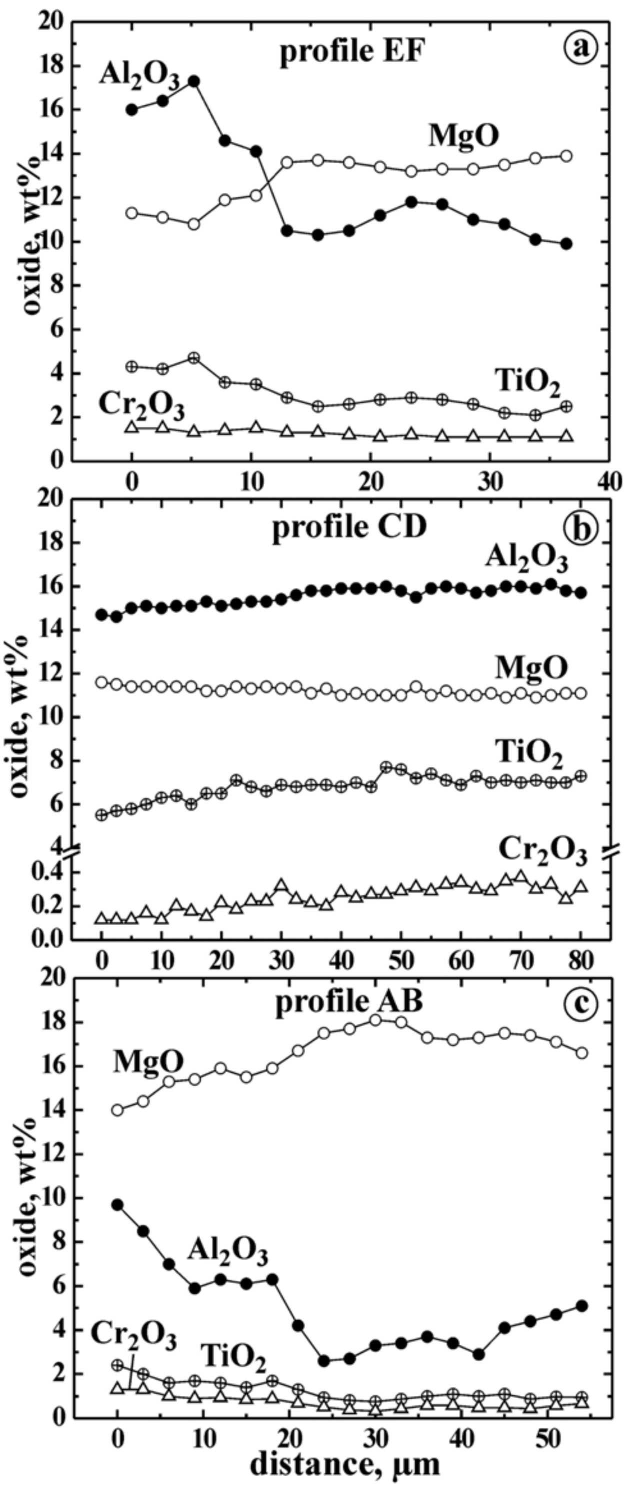

Fig. 4. Compositional profiles AB, CD, and EF across coarse Al-Ti-diopside grains in the chondrule-bearing CAI ABC. The locations of the profiles are indicated in Figs. 1d and 2b–f.

Table 3. Representative compositions of melilite in the Allende type C CAIs ABC, TS26, and 93.

Ox/CAI	ABC	ABC	TS26	93	93
SiO_2	38.1	39.5	37.8	36.9	37.6
TiO_2	0.05	0.11	0.08	<0.03	0.03
Al_2O_3	9.8	8.2	8.8	12.7	11.2
Cr_2O_3	0.01	<0.06	<0.06	<0.06	<0.06
FeO	0.87	0.36	0.54	0.57	0.36
MnO	<0.06	0.07	0.08	<0.06	<0.06
MgO	10.1	10.9	10.4	8.9	9.6
CaO	40.1	40.3	39.8	39.9	39.8
Na_2O	0.48	0.51	0.40	0.58	0.56
K_2O	<0.06	<0.06	<0.06	<0.06	<0.06
Total	99.5	99.9	98.0	99.5	99.1
Åk, mol%	68.9	73.7	72.4	68.4	72.3

however, crosscut the spinel-rich layer and occur in the pigeonite-augite-rich region, suggesting they co-crystallized with the pigeonite-augite grains (Figs. 9, 10a, 10c). The bottom left portion of the CAI consists of fine-grained, elongated crystals of diopside, augite, anorthitic plagioclase, and minor pigeonite (Figs. 9a, 10g, 10h). Both plagioclase (An_{89}) (Table 1) and augite ($Fs_{0.6 \pm 0.3}Wo_{43.2 \pm 3.2}$; [in wt%] TiO_2, 0.68 ± 0.25; Al_2O_3, 3.8 ± 1.7; Cr_2O_3, 0.53 ± 0.13) (Table 2) are compositionally similar to phases in the coarse-grained pigeonite-augite-plagioclase igneous region described above. The diopside ($Fs_{0.3}Wo_{48.0}$) is depleted in Al_2O_3 and TiO_2 and enriched in Cr_2O_3 (9.4 ± 2.1, 0.80 ± 0.06, and 0.47 ± 0.07 wt%, respectively) compared to the coarse grains in the CAI core (Table 1).

Oxygen and Magnesium Isotope Compositions

Oxygen isotope compositions of the CAIs ABC, TS26, and 93 are listed in Table 7 and plotted in Figs. 12a, 12b, and 12c, respectively. Aluminum-magnesium isotope systematics of these CAIs compositions are listed in Table 8 and shown in Fig. 13.

In ABC, olivine and pigeonite have ^{16}O-poor compositions ($\Delta^{17}O$ = −5.5‰ and −4.0‰, respectively). Spinel and Al-Ti-diopside are moderately ^{16}O-enriched ($\Delta^{17}O$ to −15.5‰). We note that there is a significant range in the oxygen isotopic compositions of the Al-Ti-diopside ($\Delta^{17}O$ = −5.6‰ to −15.5‰); both the highest and the lowest values of $\Delta^{17}O$ were found in the right portion ("mantle") of the CAI. Chromian spinel ($\Delta^{17}O$ = −10.6‰), anorthite ($\Delta^{17}O$ = −5.4‰ to −1.1‰), and melilite ($\Delta^{17}O$ = 1.8‰) are ^{16}O-depleted to varying degrees (Fig. 12a). Anorthite in ABC shows a well-resolved $^{26}Mg^*$, corresponding to a $(^{26}Al/^{27}Al)_0$ ratio of (4.7 ± 1.4) × 10^{-6} (Fig. 13).

In TS26, olivine and augite have ^{16}O-poor compositions ($\Delta^{17}O$ = −1.1‰ and −8.1‰, respectively); spinel is ^{16}O-rich (^{17}O = −19.9‰). Al-Ti-diopside ($\Delta^{17}O$ = −3.1‰ to −14.5‰) and anorthite ($\Delta^{17}O$ = −3.0‰ to 0.8‰) are ^{16}O-depleted to varying degrees (Fig. 12b). The coarse Al-Ti-diopside grains in the core are less ^{16}O-depleted compared to those in the finer-grained mantle ($\Delta^{17}O$ range from −5‰ to −14.5‰ and from −3.1‰ to −4.1‰, respectively). Anorthite, spinel, and

Table 4. Representative compositions of grossular, monticellite, wollastonite, ferrous olivine, nepheline, sodalite, sphene, and unidentified Ca-Al-Ti-silicate in the Allende type C CAIs ABC, TS26, and 93.

CAI	ABC	ABC	ABC	ABC	ABC	ABC	ABC	TS26	TS26	TS26	TS26	93	93	93	93
ox/min[a]	grs	mcl	mes	nph	sph	UNK	wol	andr[b]	grs	mcl	wol	fa	grs	mcl	sod
SiO_2	40.0	38.1	47.4	41.6	29.0	27.1	50.9	34.3	38.6	36.8	49.5	38.1	39.6	37.3	38.2
TiO_2	0.15	<0.03	0.06	<0.03	39.1	25.6	<0.03	<0.03	0.18	<0.03	<0.03	<0.03	<0.03	<0.03	<0.03
Al_2O_3	22.1	<0.04	8.7	37.3	1.1	14.1	0.29	0.52	21.8	0.19	0.20	0.16	22.5	0.07	33.9
Cr_2O_3	<0.06	<0.06	<0.06	<0.06	<0.06	<0.06	<0.06	<0.06	<0.06	<0.06	<0.06	<0.06	<0.06	<0.06	<0.06
FeO	0.49	0.51	5.2	0.11	0.08	0.94	0.12	30.7	1.0	1.1	0.16	22.9	0.24	0.74	0.22
MnO	<0.06	0.17	0.29	<0.06	0.13	0.17	<0.06	0.66	<0.06	0.16	<0.06	0.23	<0.06	0.06	<0.06
MgO	1.3	25.5	9.6	<0.03	0.15	0.81	0.41	0.06	0.48	24.5	2.1	36.7	0.55	24.5	0.46
CaO	37.2	36.1	28.5	2.2	27.6	29.7	47.1	31.8	37.1	35.6	47.0	0.14	37.5	35.7	0.17
Na_2O	<0.06	<0.06	0.19	18.2	0.07	0.37	<0.06	<0.06	<0.06	<0.06	<0.06	0.15	<0.06	<0.06	20.7
K_2O	<0.06	<0.06	<0.06	1.8	<0.06	<0.06	<0.06	<0.06	<0.06	<0.06	<0.06	<0.06	<0.06	<0.06	<0.06
Total	101.1	100.4	99.9	101.2	97.2	98.8	98.9	98.0	99.2	98.4	99.0	98.3	100.4	98.4	93.7

[a]ox = oxide; min = mineral; andr = andradite; fa = ferrous olivine; grs = grossular; mcl = monticellite; mes = fine-grained interstitial material; nph = nepheline; sod = sodalite (Cl has not been analyzed); sph = sphene; UNK = unidentified Ca-Al-Ti-silicate; wol = wollastonite.

[b]Fe as Fe_2O_3.

Table 5. Representative compositions of spinel in the Allende type C CAIs ABC, TS26, and 93.

Ox/CAI	ABC	ABC	TS26	TS26	TS26	93	93	93
SiO_2	0.05	0.04	0.05	0.06	0.06	0.05	0.03	0.05
TiO_2	0.21	0.35	0.31	0.29	0.34	0.22	0.11	0.17
Al_2O_3	70.3	68.5	71.5	66.9	66.4	71.3	69.6	66.0
Cr_2O_3	1.8	4.5	0.16	0.18	3.8	0.20	2.2	0.20
FeO	0.83	1.5	1.2	15.8	1.2	2.7	0.70	15.6
MnO	0.17	0.36	0.13	0.13	0.14	0.04	<0.06	0.11
MgO	26.9	26.6	26.5	16.4	25.7	26.2	27.4	17.0
CaO	0.06	0.07	0.11	0.06	0.16	0.03	0.06	0.10
Na_2O	<0.06	<0.06	<0.06	<0.06	<0.06	<0.06	<0.06	<0.06
K_2O	<0.06	<0.06	<0.06	<0.06	<0.06	<0.06	<0.06	<0.06
Total	100.4	102.0	99.9	99.8	97.8	100.7	100.1	99.2

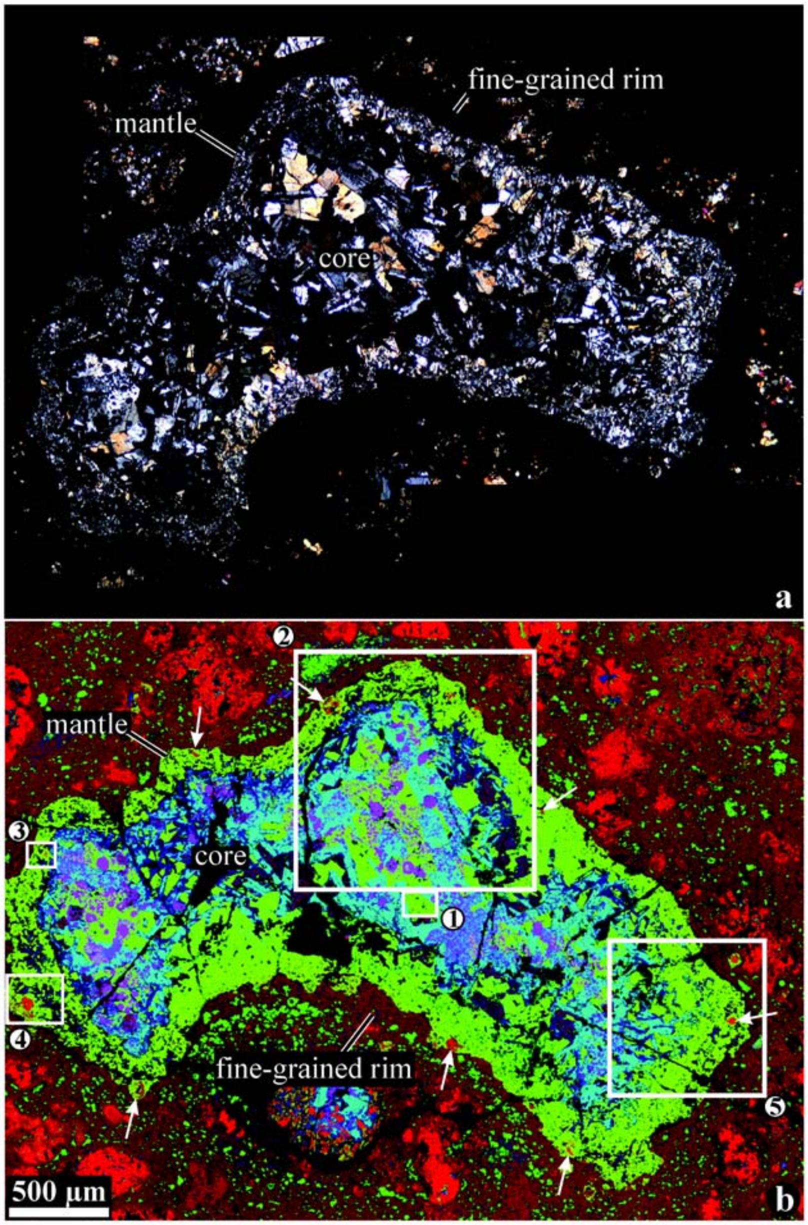

Fig. 5. a) Optical micrograph in transmitted light (cross polars) and b) combined elemental map in Mg (red), Ca (green), and Al Kα (blue) X-rays of the Allende type C CAI TS26. The CAI has a coarse-grained core and a finer-grained mantle. It is surrounded by a fine-grained matrix-like rim. The fine-grained mantle contains abundant olivine and low-Ca pyroxene grains (reddish in color; indicated by arrows in [b]). Regions outlined and numbered from 1 to 6 in (b) are shown in detail in Figs. 6, 7, and A1.

Al-Ti-diopside show no resolvable ^{26}Mg*; the upper limit on the $(^{26}Al/^{27}Al)_0$ ratio is 1.2×10^{-6} (Fig. 13).

In CAI 93, spinel shows the highest enrichment in ^{16}O (^{17}O = −15.9‰); Al-Ti-diopside is ^{16}O-depleted (Δ^{17}O = −10.7‰ to −7.8‰); anorthite and melilite are ^{16}O-poor (Δ^{17}O = −1.8‰ and −1.3‰, respectively) (Fig. 12c; Table 7). Oxygen isotopic composition of augite the coarse-grained, igneous rim (Δ^{17}O = –4.7‰ to –7.8‰) is similar to that of Al-Ti-diopside of the host CAI. Anorthite and spinel show no resolvable ^{26}Mg*; the inferred $(^{26}Al/^{27}Al)_0$ ratio is $(1.5 \pm 1.8) \times 10^{-6}$ (Fig. 13).

DISCUSSION

Relict Origin of Olivine and Low-Ca Pyroxene in ABC and TS26

The corroded appearance of olivine–low-Ca pyroxene/pigeonite fragments in ABC and TS26 and their ^{16}O-poor isotopic compositions, compared to those of the surrounding Al-Ti-diopside of the host CAIs, suggest that these grains were incorporated into the host CAI melts as solids and were partly dissolved. Since both relict minerals have no to low calcium contents, the dissolution process may have resulted in depletion of the surrounding melt in Ca and the formation of augite haloes around the fragments. The lower abundance and smaller grain sizes of low-Ca pyroxene/pigeonite compared to forsteritic olivine could be due to differences in the dissolution rates of olivine and low-Ca pyroxene in silicate melts; in ultramafic melts, forsterite dissolves much more slowly than enstatite (Kirkpatrick 1975; Kuo and Kirkpatrick 1985; Greenwood and Hess 1996). We note, however, that experimental data on dissolution rates of olivine and low-Ca pyroxene in Ca-Al–rich melts are absent.

The relict origin of the olivine-pyroxene fragments is also consistent with the absence of either olivine or low-Ca pyroxene/pigeonite in the crystallization sequence predicted from the experimental study of Stolper (1982) for melts having ABC- or TS26-like bulk composition: spinel anorthite $\rightarrow$ Al-Ti-diopside $\rightarrow$ melilite (Fig. 14). The coarse-grained nature of relict forsteritic olivine associated with Cr-bearing low-Ca pyroxene and their ^{16}O-poor compositions suggest these grains are probably fragments of ferromagnesian chondrules (Krot et al. 2006a and references therein). Although coarse olivine grains occasionally associated with low-Ca pyroxene or pigeonite are also found in AOAs and in forsterite-rich accretionary rims around CV CAIs, low-Ca pyroxene/pigeonite in these objects is Cr-poor and forms thin corrosion layers around olivine (Krot et al. 2004a, 2004d). In addition, both olivine and low-Ca pyroxene in AOAs have ^{16}O-rich compositions suggesting a condensation origin in an ^{16}O-rich gaseous reservoir, i.e., the CAI-forming region (Krot et al. 2002b, 2004b).

Remelting ABC, TS26, and 93 in the Chondrule-Forming Regions

Most coarse-grained igneous CAIs in CV chondrites show oxygen isotopic heterogeneity: spinel and Al-Ti-diopside are typically ^{16}O-rich ($\Delta^{17}O \sim -20‰$), whereas melilite and anorthite are ^{16}O-depleted to varying degrees ($\Delta^{17}O$ up to 5‰) (Clayton 1993). This heterogeneity has been attributed to oxygen isotope exchange between an ^{16}O-poor nebular gas and initially uniformly ^{16}O-rich CAIs during incomplete melting in the solar nebula (Clayton 1993; Yurimoto et al. 1998; Fagan et al. 2003; Itoh et al. 2004; Nagashima et al. 2004). Although ^{16}O-depletion in melilite and anorthite in the CAIs ABC, TS26, and 93 (Figs. 12a–c) could be partly attributed to fluid-assisted thermal metamorphism that resulted in their replacement by grossular, wollastonite, monticellite, sodalite, nepheline, and ferrous olivine (e.g., Wasson et al. 2001; Aléon et al. 2005), all three CAIs also show significant ^{16}O-depletion in Al-Ti-diopside and spinel (only in ABC) compared to typical CAIs and relict CAIs inside chondrules (Figs. 12d–f). The degree of depletion increases toward the CAI peripheries and the relict chondrule fragments that have ^{16}O-poor compositions and

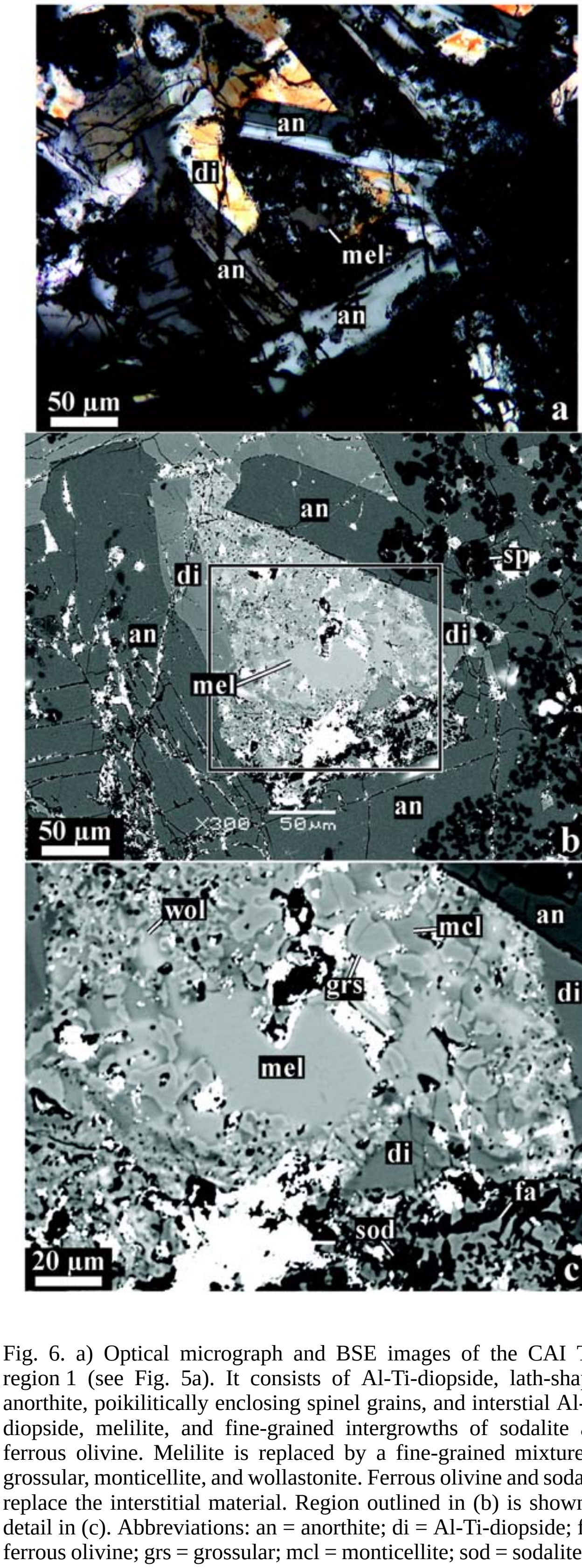

Fig. 6. a) Optical micrograph and BSE images of the CAI T26 region 1 (see Fig. 5a). It consists of Al-Ti-diopside, lath-shaped anorthite, poikilitically enclosing spinel grains, and interstial Al-Ti-diopside, melilite, and fine-grained intergrowths of sodalite and ferrous olivine. Melilite is replaced by a fine-grained mixture of grossular, monticellite, and wollastonite. Ferrous olivine and sodalite replace the interstitial material. Region outlined in (b) is shown in detail in (c). Abbreviations: an = anorthite; di = Al-Ti-diopside; fa = ferrous olivine; grs = grossular; mcl = monticellite; sod = sodalite; sp = spinel; wol = wollastonite.

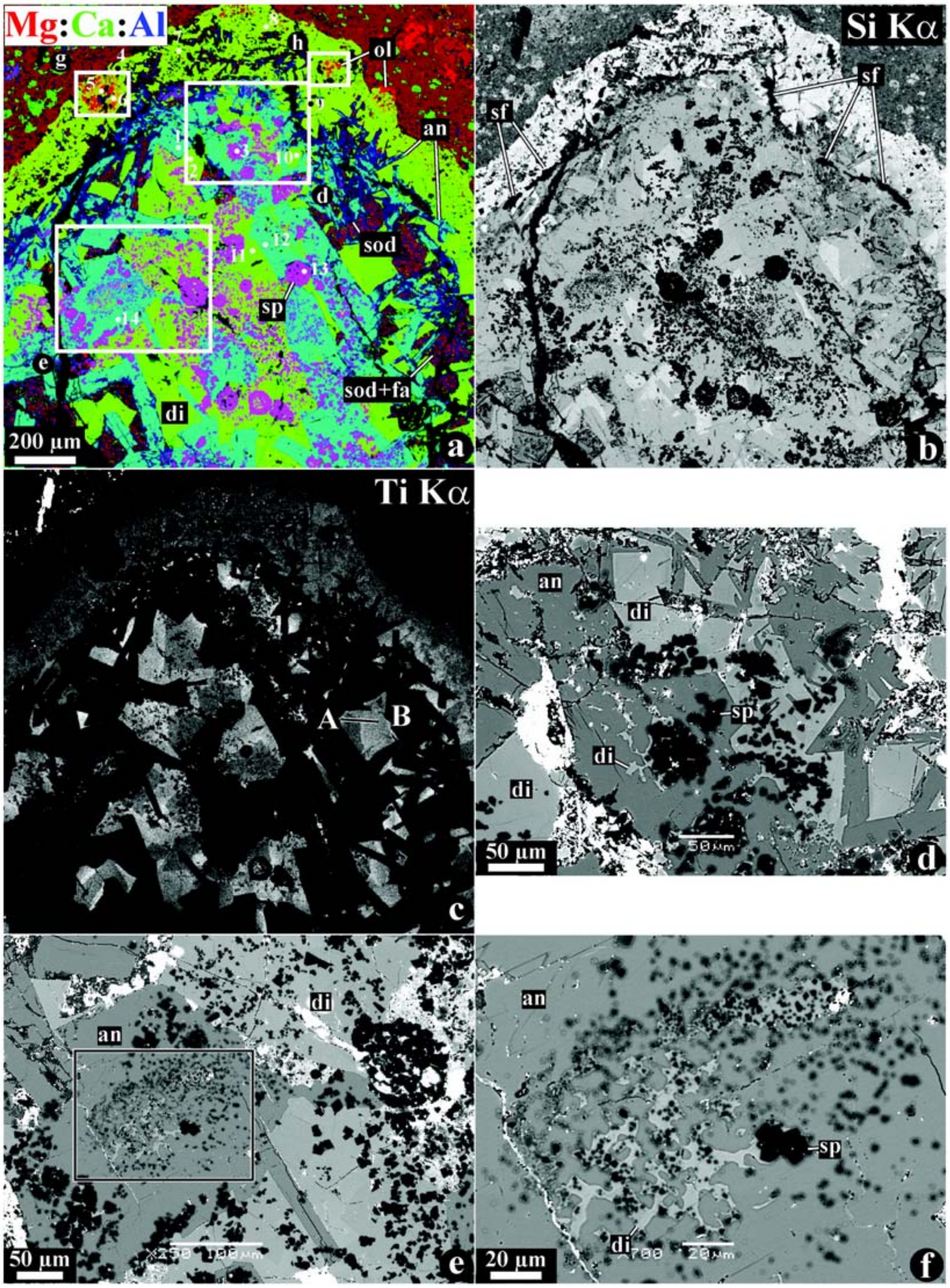

Fig. 7. a) Combined elemental map in Mg (red), Ca (green), and Al Kα (blue) X-rays, b) elemental maps in Si and c) Ti Kα, and d–j) BSE images of the CAI TS26 regions a–h) 2, i) 3, and j) 4; for locations of the regions, see Fig. 5b. Numbered white dots in (a) correspond ion probe spots of oxygen isotope analyses listed in Table 7. AB in (c) and CD in (g) indicate compositional profiles illustrated in Fig. 8. Regions outlined and labelled in (a) are shown in detail in (d), (e), (g), and (h); the region outlined in (e) is shown in detail in (f). The CAI core is composed of coarse sector-zoned Al-Ti-diopside and lath-shaped anorthite, both poikilitically enclosing spinel grains. Most of the Al-Ti-diopside grains are euhedral; rare anhedral Al-Ti-diopside grains are found inside anorthite (c–e). The CAI mantle is enriched in Si and depleted in Ti and is finer-grained than the core. It consists of Ti-poor Al-diopside and augite, lath-shaped anorthitic plagioclase, and abundant fragments of forsteritic olivine and low-Ca pyroxene/pigeonite (g–j). The fragments are heavily corroded and surrounded by haloes of augite. A discontinuous layer of Fe,Ni-sulfides occurs between the core and the mantle. Most of the bright white "grains" in BSE images are remnants of gold coating; rounded white nodules are Fe,Ni-sulfides. an = anorthite; cpx = augite; di = Al-Ti-diopside; ol = forsteritic olivine; opx = low-Ca pyroxene/pigeonite; sod = sodalite; sf = Fe,Ni-sulfides; sp = spinel.

Table 6. Compositions of relict olivine in the Allende type C CAIs ABC and TS26.

Ox/CAI	ABC	ABC	ABC	TS26	TS26	TS26	TS26
SiO_2	41.6	41.1	40.8	40.3	39.3	39.2	38.8
TiO_2	0.12	0.04	<0.03	0.04	0.07	<0.03	0.05
Al_2O_3	0.14	0.13	<0.06	<0.06	<0.06	<0.06	<0.06
Cr_2O_3	0.20	0.15	<0.06	<0.06	<0.06	<0.06	<0.06
FeO	5.5	6.7	7.5	7.9	10.8	14.2	16.4
MnO	0.18	0.16	0.16	0.17	0.12	0.21	0.15
MgO	53.2	52.0	51.3	49.7	47.8	44.9	42.8
CaO	0.28	0.35	0.28	0.41	0.30	0.46	0.30
Na_2O	<0.06	<0.06	<0.06	<0.06	<0.06	<0.06	<0.06
K_2O	<0.06	<0.06	<0.06	<0.06	<0.06	<0.06	<0.06
Total	101.2	100.7	100.3	98.6	98.5	99.0	98.6
Fa, mol%	5.5	6.8	7.6	8.1	11.2	15.1	17.7

show clear evidence for dissolution in the CAI melts. The coarse-grained igneous portion of CAI 93 composed of pigeonite, augite, and Na-bearing anorthitic plagioclase (none of these minerals are observed in typical CAIs; pure anorthite is common instead) most likely represents the melted chondrule-like material around the host CAI, analogous to coarse-grained igneous rims around chondrules (e.g., Krot and Wasson 1995). Based on these observations, we infer that ABC, TS26, and 93 experienced oxygen isotope exchange during melting in a ^{16}O-poor gas, probably in the chondrule-forming region. The outer portions of these CAIs were also diluted by ^{16}O-poor relict ferromagnesian chondrule-like silicate materials.

The observed differences in grain sizes between the core and the mantle of TS26 (Figs. 5, 7, and A1) suggest that melting was incomplete and followed by relatively fast cooling. A fine-grained region composed of prismatic Al-diopside, augite, and anorthitic plagioclase in CAI 93 (Figs. 10g and 10h) could also imply fast cooling during remelting. The absence of Wark-Lovering rim layers around TS26 and 93 could be due to the inferred melting episode as well. The high abundance of relict chondrule-like material in the outer portion of TS26 (Fig. 5b) and the presence of coarse-grained, chondrule-like igneous rim around 93 (Figs. 9 and 10) suggest there was a high abundance of dust in the region where melting occurred, which is consistent with the dusty environment inferred for chondrule formation (Desch and Connolly 2002).

Other examples of CAIs remelted in the chondrule-forming region include relict CAIs inside chondrules (Misawa and Nakamura 1988; Maruyama et al. 1999; Krot and Keil 2002; Krot et al. 1999, 2001b, 2002c, 2004c; Maruyama and Yurimoto 2003; Russell et al. 2005) and ^{16}O-depleted type C CAIs in the CR carbonaceous chondrites (Krot et al. 2005a). Relic CAIs in chondrules preserved their ^{16}O-rich signature to varying degrees, depending on the degree of melting and assimilation by the host chondrule material (Figs. 12d–f). Two type C CAIs in CR chondrites contain no associated chondrule material, but

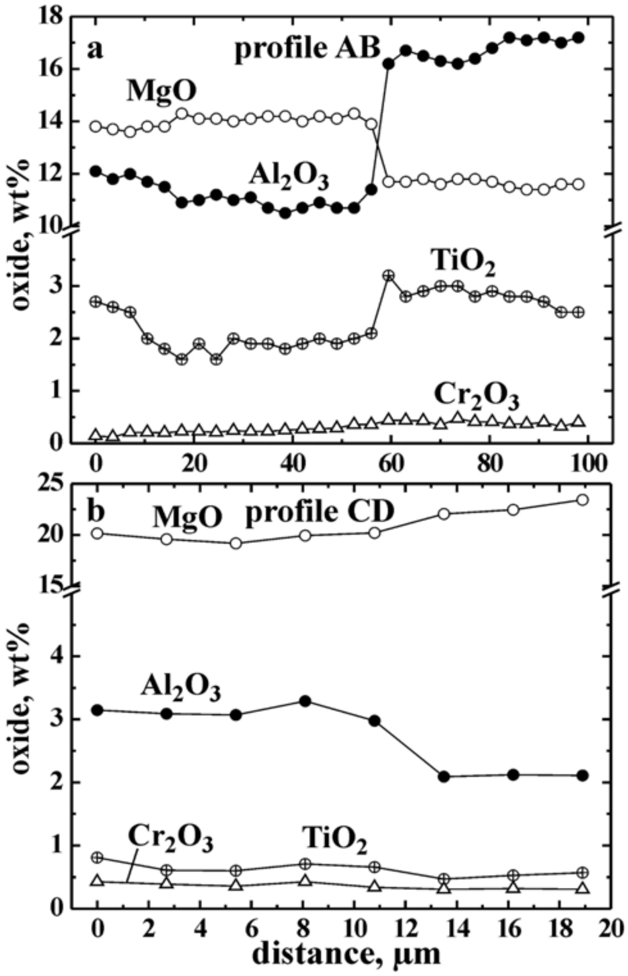

Fig. 8. a) Compositional profiles across sector-zoned Al-Ti-diopside grain in the core of CAI TS26 core b) and augite in its mantle. The positions of the compositional profiles are shown in Figs. 7c and 7g.

are ^{16}O-depleted to a level observed in the CR chondrules (Fig. 12e) and have low initial $^{26}Al/^{27}Al$ ratios (Krot et al. 2005a).

Further Evidence for Multistage Formation History of ABC, TS26, and 93

There are several observations suggesting that ABC, TS26, and 93 may have experienced multiple melting events prior to incorporation of ferromagnesian chondrule-like fragments (ABC, TS26) and formation of ferromagnesian chondrule-like igneous rim (93).

1. ABC is characterized by a bi-modal distribution of Al-Ti-diopside chemical compositions: Al-Ti-diopside in the mantle zone is significantly enriched in moderately volatile chromium relative to the core and show oscillatory zoning (Figs. 1 and 3a). Because such high Cr contents cannot be explained by incorporation of chondrule material present as relict grains, which are Cr-

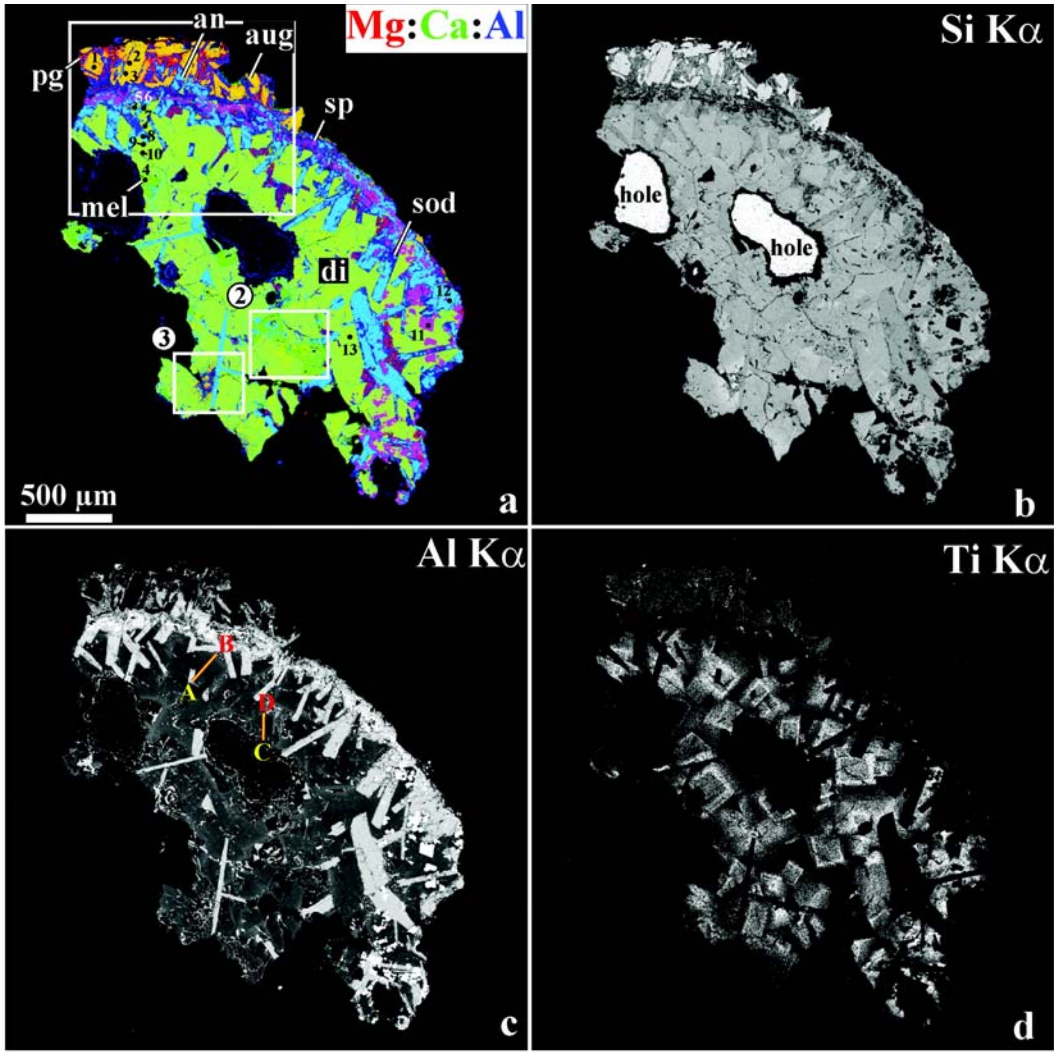

Fig. 9. a) Combined elemental map in Mg (red), Ca (green), and Al Kα (blue) X-rays and elemental maps in b) Si, c) Al, and d) Ti Kα of a type C CAI 93 from Allende. Regions outlined and numbered as 1, 2, and 3 in (a) are shown in detail in Figs. 10a, 10d, and 10g, respectively. Numbered dots in (a) correspond ion probe spots of oxygen isotope analyses listed in Table 7. The CAI consists of lath-shaped anorthite, melilite, highly åkermanitic melilite, oscillatory zoned Al-Ti-diopside, and spinel. Anorthite is replaced by nepheline, sodalite, and ferrous olivine (see Figs. 10b and 10c for details). Top left portion of the CAI is intergrown with a coarse-grained igneous region composed of low-Ti augite, pigeonite, and anorthitic plagioclase. The CAI is separated from this region by a spinel-rich layer, which may represent remnant of a Wark-Lovering rim. Anorthite crystals are oriented away from the spinel-rich layer toward the CAI core; some of them crosscut the spinel-rich layer. an = anorthite and anorthitic plagioclase; aug = augite; di = diopside; mel = melilite; pg = pigeonite; sod = sodalite; sp = spinel.

poor (Fig. 3a), we infer that Cr could have been added either by condensation into CAI melt or with Cr-rich solids which were completely melted. Both events may have occurred prior to incorporation of the relict olivine and low-Ca pyroxene.

2. It is generally believed that both nonigneous and igneous CAIs were originally uniformly ^{16}O-rich and experienced O-isotope exchange to various degree during subsequent melting event(s) (e.g., Yurimoto et al. 1998). Coarse Al-Ti-diopside grains in the core of TS26 are ^{16}O-enriched relative to the finer-grained Al-Ti-diopside of its mantle; the former, however, are not as ^{16}O-rich as co-existing spinel (Fig. 12b). Based on these observations, we infer that some oxygen isotope exchange of the core Al-Ti-diopside may have occurred prior to the melting event that produced the TS26 mantle.

3. All three CAIs contain very Na-rich melilite in their cores (Fig. 15), suggesting addition of Na to the protoCAIs either during alteration prior to (MacPherson and Davis 1993) or during melting (Krot et al. 2004e). MacPherson and Davis (1993), MacPherson (2003), and Beckett et al. (2000) suggested that high Na contents in melilite of coarse-grained CAIs in CV chondrites resulted from replacement of melilite and anorthite by nepheline and sodalite during high-temperature gas-

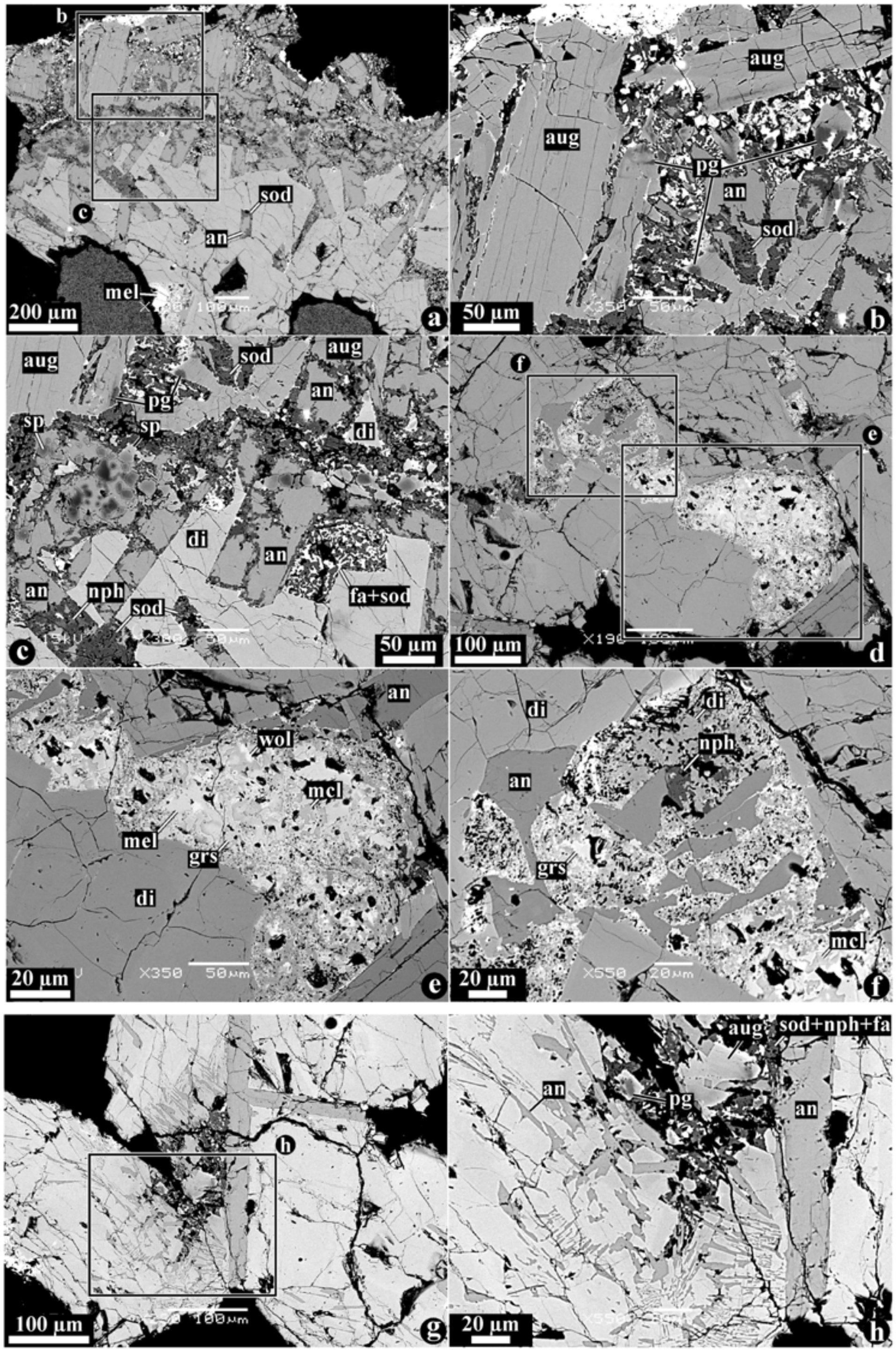

Fig. 10. a–f) BSE images of the Allende CAI 93. Regions outlined in (a), (d), and (g) are shown in detail in (b), (c), (e), (f), and (h), respecitively. a–c) Coarse-grained, igneous region composed of prismatic igneously zoned pigeonite-augite crystals and anorthitic plagioclase partly replaced by sodalite, nepheline, and ferrous olivine. This igneously zoned region is separated from the CAI by a spinel-rich layer. The spinel grains are enriched in FeO to various degrees. The CAI core consists largely of coarse-grained Al-Ti-diopside and lath-shaped anorthite. Some of the coarse anorthite crystals in the CAI periphery crosscut the spinel-rich layer and appear to have co-crystallized with the pigeonite-augite grains. d–f) The interstitial regions between Al-Ti-diopside and anorthite crystals in the CAI core consist of fine-grained melilite, anorthite, and Al-diopside, which are replaced by grossular, wollastonite, monticellite, sodalite, and nepheline. g–h) Fine-grained region composed of diopside, augite, pigeonite, and anorthitic plagioclase; the latter is replaced by nepheline, sodalite, and ferrous olivine. Abbreviations: an = anorthite and anorthitic plagioclase; aug = augite; di = diopside; fa = ferrous olivine; grs = grossular; mel = melilite; mcl = monticellite; nph = nepheline; pg = pigeonite; sod = sodalite; sp = spinel; wol = wollastonite.

Table 7. Oxygen isotope compositions of individual minerals in the chondrule-bearing CAIs ABC, TS26, and 93.

Spot no.	Mineral	$\delta^{17}O$	2σ	$\delta^{18}O$	2σ	$\Delta^{17}O$	2σ
ABC							
1	An[a]	–2.3	3.3	6.0	2.0	–5.4	3.9
2	Sp	–29.2	2.4	–28.2	3.0	–14.5	3.9
3	Al-Ti-di, core	–28.6	2.5	–28.4	3.1	–13.8	4.0
4	Al-Ti-di, core	–22.1	2.5	–22.6	3.1	–10.4	4.0
5	Al-Ti-di, core	–20.2	2.5	–20.2	3.1	–9.7	4.0
6	Al-Ti-di, mantle	–27.2	2.5	–28.7	3.1	–12.3	4.0
7	Al-Ti-di, mantle	–30.6	2.5	–29.1	3.1	–15.5	4.0
8	Al-Ti-di, mantle	–15.2	2.5	–14.0	3.1	–7.9	4.0
9	Al-Ti-di, mantle	–11.9	2.5	–12.2	3.1	–5.6	4.0
10	Ol	–8.2	1.5	–5.1	2.1	–5.5	2.6
11	Px	–8.1	2.5	–7.9	3.1	–4.0	4.0
12	An	–0.2	3.3	5.8	2.0	–3.2	3.9
13	Cr-sp	–21.8	2.4	–21.6	3.0	–10.6	3.9
14	Al-Ti-di, core	–27.5	2.5	–28.4	3.1	–12.7	4.0
15	Mel	3.1	2.8	2.5	4.1	1.8	5.0
16	Al-Ti-di, core	–27.2	2.5	–30.1	3.1	–11.6	4.0
17	An	2.5	3.3	7.0	2.0	–1.1	3.9
TS26							
1	An	–3.2	2.2	–0.4	3.2	–3.0	3.9
2	Al-Ti-di, core	–26.9	2.2	–23.9	3.2	–14.5	3.9
3	Sp	–43.4	2.2	–46.7	3.2	–19.2	3.9
4	Al-Ti-di, mantle	–7.4	2.2	–6.3	3.2	–4.1	3.9
5	Ol	–3.3	2.2	–4.3	3.2	–1.1	3.9
6	Aug	–9.4	2.2	–2.6	3.2	–8.1	3.9
7	Al-Ti-di, mantle	–6.1	2.2	–5.5	3.2	–3.3	3.9
8	Al-Ti-di, mantle	–6.0	2.2	–5.6	3.2	–3.1	3.9
9	Al-Ti-di, core	–11.0	2.2	–11.7	3.2	–5.0	3.9
10	Al-Ti-di, core	–23.0	2.2	–24.5	3.2	–10.3	3.9
11	Al-Ti-di, core	–21.7	2.2	–23.0	3.2	–9.8	3.9
12	An	4.1	2.2	5.4	3.2	1.3	3.9
13	Sp	–44.4	2.2	–47.2	3.2	–19.9	3.9
14	An	3.3	2.2	4.9	3.2	0.8	3.9
93							
1	Aug	–9.5	0.7	–3.3	0.7	–7.8	0.8
2	Aug	–6.1	0.6	–2.6	0.7	–4.7	0.7
3	Aug	–8.4	0.6	–2.8	0.8	–7.0	0.7
4	Mel	6.3	0.6	14.5	0.8	–1.3	0.8
5	Al-Ti-di + an + sec	–13.7	0.8	–6.9	0.8	–10.1	0.9
6	Al-Ti-di + an	–4.3	0.6	–1.4	0.8	–3.6	0.7
7	Al-Ti-di	–15.5	0.7	–10.5	0.7	–10.1	0.8
8	An + sec	3.8	0.6	8.7	0.8	–0.8	0.7
9	Al-Ti-di + an	–11.9	0.6	–9.6	0.7	–6.9	0.7
10	Al-Ti-di	–12.7	0.6	–9.5	0.8	–7.8	0.7
11	Sp	–33.8	0.6	–34.4	0.7	–15.9	0.7
12	An	1.3	0.6	5.9	0.8	–1.8	0.7
13	Al-Ti-di	–15.7	0.7	–9.4	0.8	–10.7	0.8

[a]an = anorthite; aug = augite; Al-Ti-di = Al-Ti-diopside; Cr-sp = chromian spinel; mel = melilite; ol = olivine; pg = pigeonite; px = pigeonite + augite; sec = secondary minerals; sp = spinel.

solid reactions, followed by melting. Since most CAIs in CV chondrites are characterized by canonical $^{26}Al/^{27}Al$ ratios, this scenario would require alteration to have occurred very early. This time scale is, however, difficult to reconcile with the general lack of $^{26}Mg^*$ in sodalite and nepheline and their ^{16}O-poor compositions (e.g., MacPherson et al. 1995; Fagan et al. 2006; Krot et al. 2006b). In addition, it has been suggested that nepheline and sodalite formed during fluid-assisted thermal metamorphism on the CV parent body, not in the solar nebula (Krot et al. 1995, 1998; Nomura and Miyamoto 1998).

An alternative mechanism for the introduction of Na into coarse-grained igneous CAIs is through gas-melt interaction. Based on the mineralogical studies of chondrules in primitive ordinary and carbonaceous chondrites (Libourel et al. 2002; Krot et al. 2004f), and the experiments on gas-melt interaction (Tissandier et al. 1999), it was suggested that silica and alkalis condensed into chondrule melts in regions with enhanced partial pressure of silica and alkalis and/or high total pressure dust/gas ratio (Libourel et al. 2002; Alexander 2003; Krot et al. 2004f; Davis et al. 2005; Cuzzi and Alexander 2006). The fact that melilite grains in chondrule-bearing type C CAIs have much higher Na contents than those in other type C CAIs (Fig. 15) may support addition of Na through gas-melt interaction during remelting in the chondrule-forming region.

All three type C CAIs studied here experienced postcrystallization alteration that resulted in replacement of primary minerals by grossular, monticellite, wollastonite, sodalite, nepheline and ferrous olivine. Grossular, monticellite, and wollastonite are observed in interstitial regions between Al-Ti-diopside and anorthite and appear to have replaced melilite and anorthite (Figs. 2a–c, 6, 10d–f). Nepheline and sodalite replace anorthite or anorthitic plagioclase (Figs. 1a, 1f, 2f, 7i, 10a, 10f). Ferrous olivine typically forms intergrowths with sodalite (Figs. 6b, 6c, 10c). The enrichment of spinel and relict olivine grains in FeO most likely resulted from iron-alkali metasomatic alteration that affected all components of the Allende meteorite (e.g., Krot et al. 1998).

Based on petrographic observations and thermodynamic analysis, Hutcheon and Newton (1981) concluded that grossular and monticellite formed during prolonged heating in the solar nebula at ~950 K via the closed-system reaction:

$$3Ca_2MgSi_2O_7 + Ca_2Al_2SiO_7 + CaAl_2Si_2O_8 = 2Ca_3Al_2Si_3O_{12} + 3CaMgSiO_4 \quad (1)$$

However, based on the common presence of unaltered melilite-anorthite intergrowths in Allende type C CAIs, Krot et al. (2004e) inferred that this reaction could have occurred under disequilibrium conditions at lower temperatures (<750 K), e.g., at the peak metamorphic temperatures experienced by Allende (~400–500 °C) (Krot et al. 1995, 1998 and references therein). Our petrographic observations suggest that wollastonite was also produced during this alteration process and appears to have predated formation of iron and alkali-rich secondary minerals during an open-system alteration, in agreement with Krot et al. (2004e) and Fagan et al. (2004):

$$4Ca_2MgSi_2O_7 + Ca_7Al_7SiO_7 + CaAl_7Si_7O_8 = 2Ca_3Al_7Si_3O_{12} + 4CaMgSiO_4 + CaSiO_3 \quad (2)$$

Timing of Remelting of ABC, TS26, and 93

The low $(^{26}Al/^{27}Al)_0$ ratios observed in ABC, TS26, and 93 (Fig. 13) may record the timing of late-stage remelting during which chondrule fragments were incorporated into the CAIs. We note, however, that because Allende experienced thermal metamorphism (Krot et al. 1998; Bonal et al. 2006) that may have disturbed the ^{26}Al-^{26}Mg systematics in CAIs and chondrules (LaTourrette and Wasserburg 1998; Yurimoto et al. 2000), apparent age differences between the formation of CAIs ABC and TS26 and their remelting should be considered with caution. The proposed multistage formation history of ABC and TS26 is consistent with the extended (~2 Myr) formation time of several other igneous CAI from CV chondrites inferred from the range of the $(^{26}Al/^{27}Al)_0$ ratios within a single inclusion and petrographic observations (MacPherson and Davis 1993; Hsu et al. 2000). Late-stage melting and oxygen isotopic exchange of ABC and TS26 are also consistent with a recently proposed model for the global evolution of the oxygen isotope composition of the inner solar nebula gas from ^{16}O-rich to ^{16}O-poor with time (Yurimoto and Kuramoto 2004; Krot et al. 2005a).

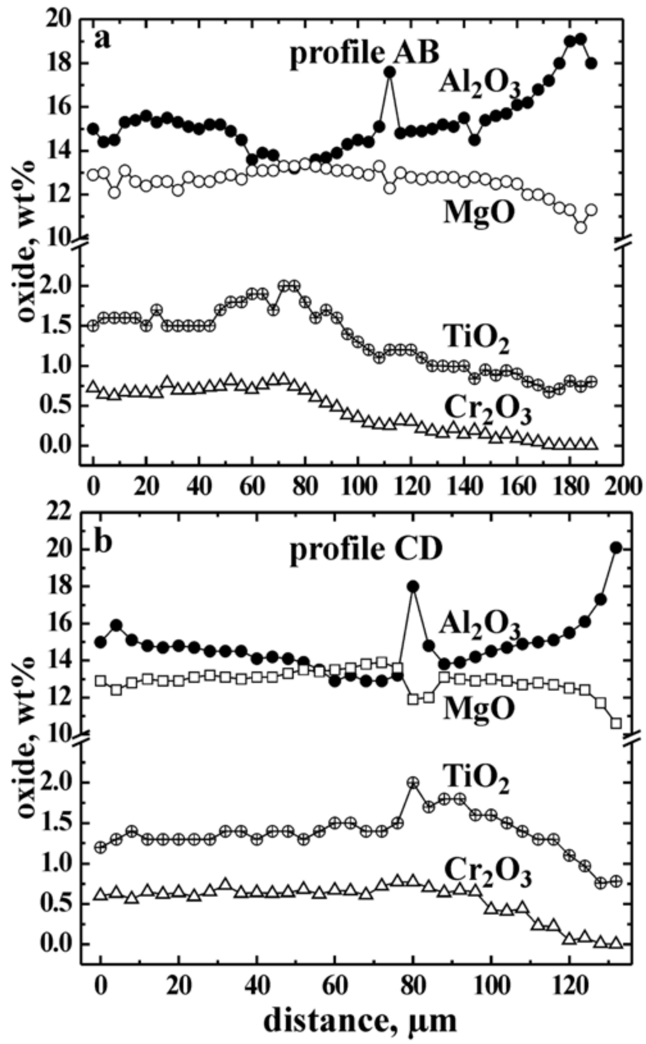

Fig. 11. Compositional profiles across coarse Al-Ti-diopside grains of the CAI #93; the positions of the compositional profiles are shown in Fig. 9c.

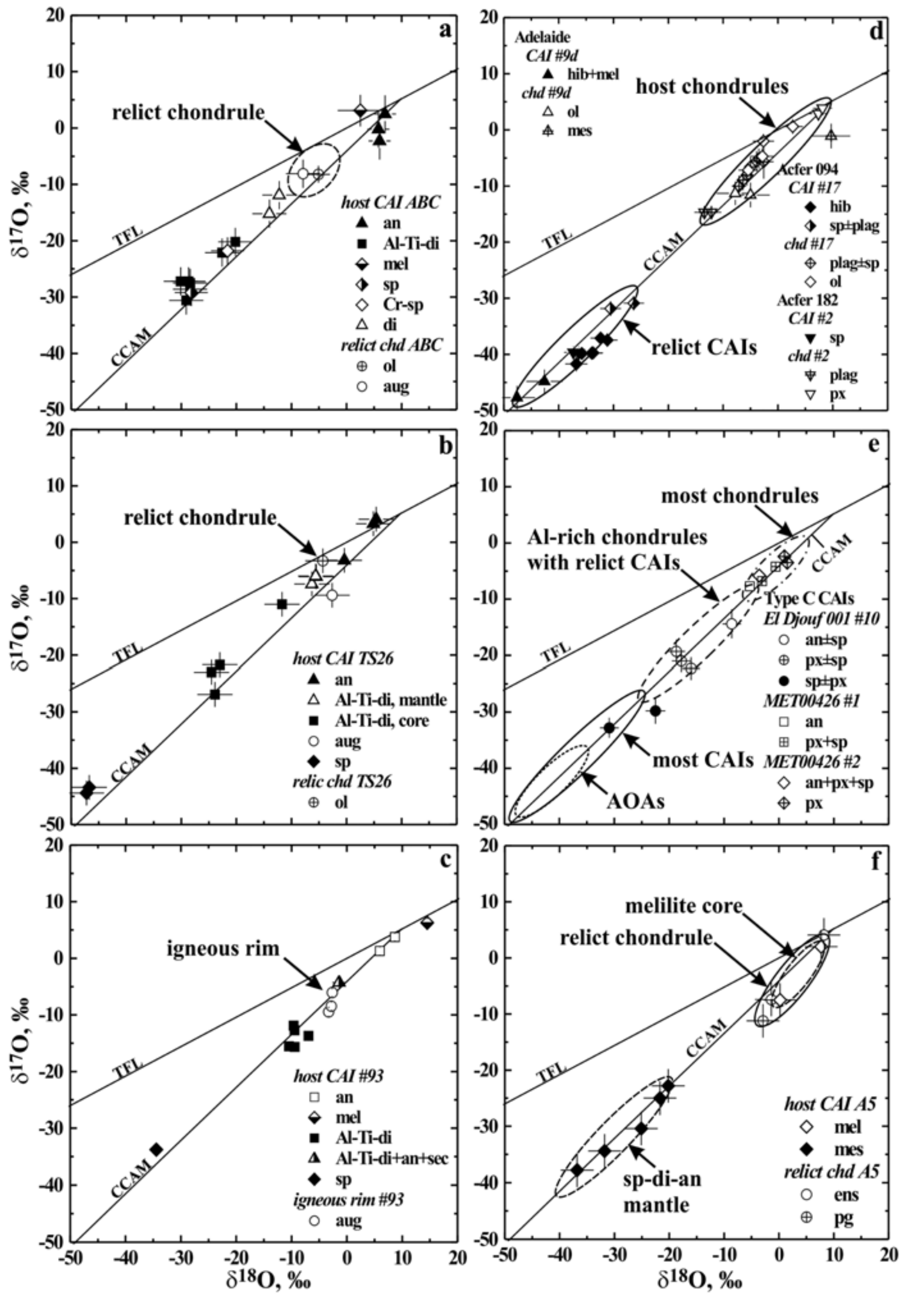

Fig. 12. Oxygen isotopic compositions of the chondrule-bearing type C CAIs a) ABC and b) TS26, c) CAI 93 surrounded by a chondrule-like igneous rim from Allende, d) CAI-bearing chondrules (data from Krot et al. 2005b), e) refractory inclusions and chondrules from CR chondrites (data from Aléon et al. 2002 and Krot et al. 2005b), and f) the chondrule-bearing CAI A5 from Y-81020 (data from Itoh and Yurimoto 2003). a) CAI ABC. Relict olivine and augite halo around it have ^{16}O-poor compositions. Spinel and Al-Ti-diopside of the host CAI are ^{16}O-enriched, whereas Cr-spinel, Al-Ti-poor diopside, anorthite, and melilite are ^{16}O-depleted to various degrees. b) CAI TS26. Relict olivine and augite halo around it have ^{16}O-poor compositions. Spinel of the CAI core is ^{16}O-rich, whereas Al-Ti-diopside and anorthite are ^{16}O-depleted to various degrees. The Al-Ti-diopside grains in the core are less ^{16}O-depleted compared to those in the mantle. c) CAI 93. Spinel of the CAI is ^{16}O-enriched, whereas Al-Ti-diopside, anorthite, and melilite are ^{16}O-depleted to various degrees. Augite of the chondrule-like, igneous rim is ^{16}O-depleted relative to spinel and Al-Ti-diopside of the CAI host. d) Relict CAIs are ^{16}O-enriched relative to their host chondrules. e) AOAs and most CAIs in CR chondrites are uniformly ^{16}O-rich. Chondrules without relict grains are uniformly ^{16}O-poor. Aluminum-rich chondrules with relict CAIs show oxygen isotope heterogeneity with relict grains ^{16}O-enriched relative to chondrule phenocrysts. Three type C CAIs are ^{16}O-depleted to a level observed in CR chondrules. f) CAI A5. Chondrule fragments and compact melilite core of the host CAI are ^{16}O-depleted relative to its fine-grained, porous, spinel-diopside-anorthite mantle; the latter is ^{16}O-depleted relative to typical ^{16}O-rich CAIs and AOAs in primitive chondrites (see [d] and Itoh et al. 2004). Abbreviations: Al-Ti-di = Al-Ti-diopside; an = anorthite; aug = augite; di = Al- and Ti-poor diopside; mel = melilite; ol = olivine; px = a mixture of augite (~70%) and low-Ca pyroxene (~30%); sp = spinel; CCAM = carbonaceous chondrite anhydrous mineral line. Terrestrial fractionation line and CCAM line are shown for reference.

Table 8. Aluminum-magnesium isotopic data for the Allende type C CAIs associated with chondrule-like materials.

CAI/min	$^{27}Al/^{24}Mg$	2σ	$\delta^{26}Mg$(‰)	2σ
93				
An[a]	220.0	20.0	3.8	3.1
An	195.0	10.0	0.4	3.0
An	218.0	15.0	2.6	2.6
Sp	2.5	0.1	1.6	2.0
Sp	2.5	0.1	0.4	1.5
TS26				
An	157	13	–2.3	4.3
An	207	20	–0.5	4.6
Di	1	0.1	–1.1	2.6
Di	1	0.1	–0.2	1.7
Di	1	0.1	–0.6	1.8
ABC				
An	351	28	15	6
An	276	20	12	6
Di	1.2	0.1	2.5	1.3
Pg	403	38	14	5
Pg	266	25	7	5
Sp	2.5	0.1	3.1	1.5

[a]an = anorthite; di = Al,Ti-diopside; pg = pigeonite; sp = spinel.

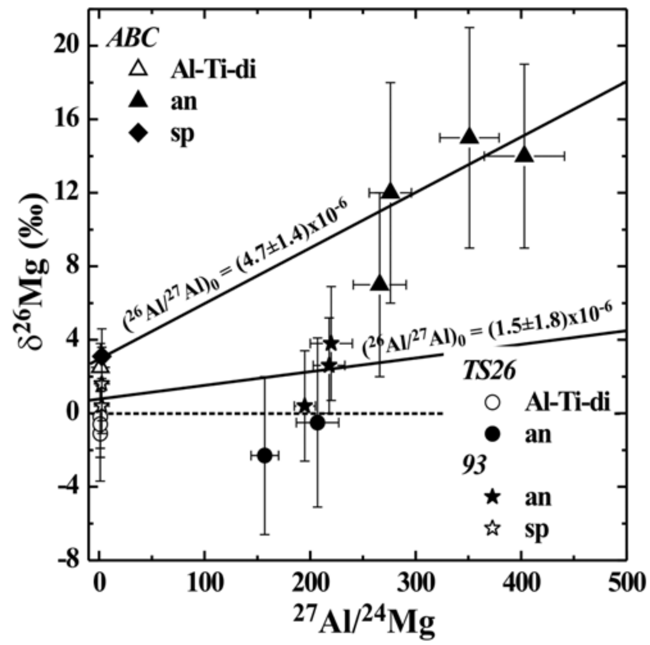

Fig. 13. Aluminum-magnesium evolution diagram for the type C CAIs ABC, TS26, and 93. ABC shows a resolvable $^{26}Mg^*$ corresponding to a $(^{26}Al/^{27}Al)_0$ ratio of (4.7 ± 1.4) × 10^{-6}. No resolvable $^{26}Mg^*$ was found in 93 and TS26; the $(^{26}Al/^{27}Al)_0$ ratios are (1.5 ± 1.8) × 10^{-6} and <1.2 × 10^{-6}, respectively. If the differences in the slopes of the correlation lines is attributed to differences in times of formation, ABC crystallized at least 1.4 Myr prior to TS26 and 93.

Origin of Chondrule-Bearing CAI A5 from Yamato-81020

Our conclusion that chondrule-bearing igneous CAIs in Allende experienced late-stage remelting in the chondrule-forming region differs from the model proposed by Itoh and Yurimoto (2003) for the origin of the chondrule-bearing CAI compact type A inclusion A5 from the CO3.0 carbonaceous chondrite Y-81020 (Fig. A2). Based on i) the inverse oxygen isotope zoning of A5, an ^{16}O-depleted coarse-grained melilite core ($\Delta^{17}O$ = 0 to –10‰) surrounded by an ^{16}O-enriched, very fine-grained Al-diopside-anorthite mantle ($\Delta^{17}O$ = –12‰ to –19‰) (Fig. 12c), and ii) the presence of enstatite-pigeonite-augite chondrule fragments inside the outer portion of A5, Itoh and Yurimoto (2003) concluded that A5 experienced remelting in an ^{16}O-rich gas in the CAI-forming region during or after addition of ^{16}O-poor chondrule-like material[3]. Below we discuss an alternative interpretation for these observations.

We note that i) the core and the mantle of A5 consist of minerals having very different rates of oxygen self-diffusion (Ryerson and McKeegan 1994) and different porosities (Fig. A2), ii) the fine-grained mantle shows a large range of oxygen isotopic compositiond and is ^{16}O-depleted relative to the vast majority of the refractory inclusions in Y-81020 (Itoh et al. 2004), and iii) the CAI lacks Wark-Lovering rim layers. Because melilite or melilite-rich melt is expected to exchange oxygen isotopes with an external reservoir much faster than spinel, diopside, anorthite (Ryerson and McKeegan 1994), or a diopside-anorthite-spinel-normative melt (Greenwood 2004), it seems possible that the inverse oxygen isotope zoning of A5 resulted from incomplete oxygen isotope exchange of the CAI during remelting in an ^{16}O-poor gas concurrent with addition of chondrule-like material, i.e., in the chondrule-forming region. Incorporation of relict pyroxene grains into A5 in the CAI-forming region characterized by high ambient temperature (at or above condensation temperature of forsterite) is inconsistent with the lack of evidence for evaporation of these grains; one of the pyroxene grains even contains inclusiond of troilite (Fig. A2). In contrast, remelting of A5 in the chondrule-forming region is consistent with fast cooling rate (>100 °C/hr) during solidification of the fine-grained mantle (Itoh and Yurimoto 2003). Such fast cooling rates are typical for chondrule melts (Desch and Connolly 2002), whereas the estimated cooling rates during crystallization of coarse-grained igneous CAIs are typically much slower (<10 °C/hr) (Davis and MacPherson 1996). If this interpretation is correct, the origin of A5 is not different from that of the chondrule-bearing type C CAIs discussed above.

[3]We note that contrary to the chondrule-bearing CAIs ABC and TS26 from Allende, the relict pyroxene grains in the outer zone of A5 show no evidence for being melted together with the host CAI, suggesting that they were probably injected into the CAI during or even after its solidification. If the latter is correct, A5 is not a truly compound object.

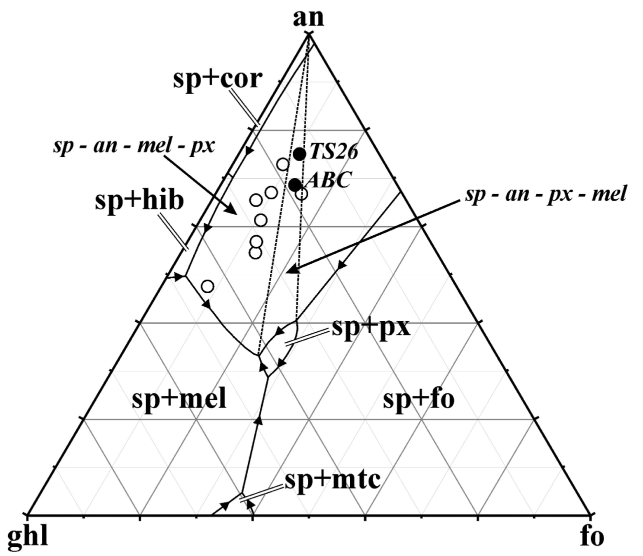

Fig. 14. Bulk compositions of the Allende type C CAIs projected from spinel onto the plane anorthite (an) forsterite (fo) gehlenite (ghl). cor = corundum; hib = hibonite; mtc = monticellite; px = Al-diopside; sp = spinel. The inferred crystallization sequence of the chondrule-bearing type C CAIs ABC and TS26 is spinel → anorthite → Al-diopside → melilite. Neither forsterite nor low-Ca pyroxene could crystallize from melts of such compositions (data from Wark 1987).

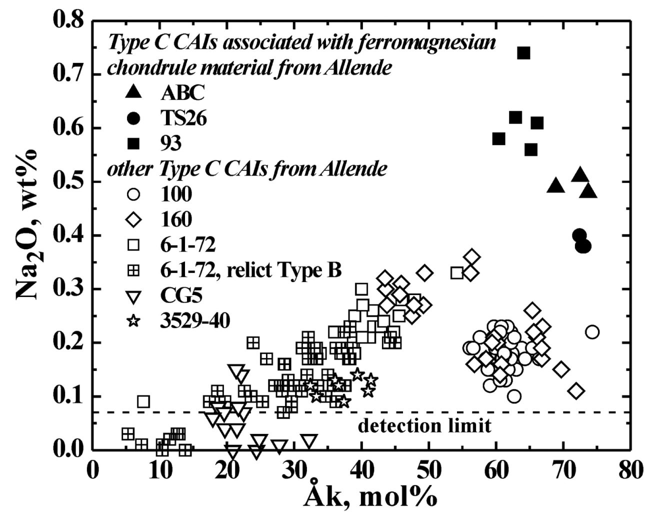

Fig. 15. Åkermanite (mol%) versus Na_2O (wt%) contents in melilite of type C CAIs from Allende. Melilite grains in chondrule-bearing type C CAIs ABC and TS26, and type C CAI 93 overgrown by a coarse-grained igneous rim have high åkermanite and Na_2O contents. Dashed line represent the detection limit of Na_2O by electron probe microanalysis.

CONCLUSIONS

1. The outer portions of the coarse-grained, igneous, anorthite-rich (type C) CAIs ABC and TS26 in Allende contain relict grains of forsteritic olivine and low-Ca pyroxene, extensively corroded by Al-Ti-diopside of the host CAI and surrounded by haloes of augite. Another type C CAI from Allende, 93, is intergrown with coarse-grained pigeonite, augite, and anorthitic plagioclase. The Al-Ti-diopside in ABC, TS26, and 93 is ^{16}O-depleted (Δ^{17}O up to −5‰) compared to typical, ^{16}O-rich (Δ^{17}O ~ −20‰) CAIs in primitive carbonaceous chondrites; relict olivine and low-Ca pyroxene/pigeonite are ^{16}O-poor (Δ^{17}O ~ −1‰ to −5‰). Contrary to typical type B CAIs in Allende having the canonical initial ^{26}Al/^{27}Al ratio of $\sim 5 \times 10^{-5}$, the three type C CAIs are ^{26}Al-poor with $(^{26}Al/^{27}Al)_0$ ratios are $(4.7 \pm 1.4)\ 10^{-6}$, $(1.5 \pm 1.8) \times 10^{-6}$, and $<1.2 \times 10^{-6}$, respectively.
2. Based on the mineralogical observations and oxygen and magnesium isotope measurements, we conclude that ABC, TS26, and 93 experienced remelting with addition of chondrule ferromagnesian silicates and incomplete oxygen isotopic exchange in an ^{16}O-poor gaseous reservoir, probably in the chondrule-forming region. This melting episode may have reset the ^{26}Al-^{26}Mg systematics of the host CAIs, suggesting it occurred ~2 Myr after formation of CAIs with the canonical ^{26}Al/^{27}Al ratio.
3. These observations and the common presence of relict CAIs inside chondrules suggest that CAIs predated chondrules and that at least some CAIs were present in the chondrule-forming regions and were affected by chondrule-melting events. That many CAIs show no evidence of being affected by chondrule heating may suggest that chondrule-forming was highly localized.

Acknowledgments–We thank Dr. Y. Guan, Dr. M. Kimura, and Dr. H. Nagahara for their comprehensive reviews, numerous comments, and suggestions, which helped to improve the manuscript. We also thank associate editor Hiroko Nagahara for handling this paper. The thin section of Allende CAI TS26 was kindly provided by Dr. L. Grossman (The University of Chicago). This work was supported by NASA grants NAG5-10610 (A. N. Krot, P.I.), NAG5-11591 (K. Keil, P.I.), NNH04AB47I (I. D. Hutcheon, P.I.), NAG5-10468 (G. J. MacPherson, P.I.), and Monkasho grants (H. Yurimoto, P.I.). This work was performed under the auspices of the U.S. Department of Energy by the University of California, Lawrence Livermore National Laboratory under Contract no. W-7405-Eng-48. This is Hawai‘i Institute of Geophysics and Planetology publication no. 1503 and School of Ocean and Earth Science and Technology publication no. 7192.

Editorial Handling—Dr. Hiroko Nagahara

REFERENCES

Aléon J., Krot A. N., and McKeegan K. D. 2002. Ca-Al-rich inclusions and amoeboid olivine aggregates from the CR carbonaceous chondrites. *Meteoritics & Planetary Science* 37: 1729–1755.

Aléon J., Krot A. N., McKeegan K. D., MacPherson G. J., and Ulyanov A. A. 2005. Fine-grained, spinel-rich inclusions from the reduced CV chondrite Efremovka: II. Oxygen isotopic compositions. *Meteoritics & Planetary Science* 40:1043–1058.

Alexander C. M. O'D. 2003. Meteoritics: A question of timing. *Nature* 423:691–692.

Alexander C. M. O'D. 2005. Chemical equilibrium and kinetic constraints for chondrule and CAI formation conditions. *Geochimica et Cosmochimica Acta* 68:3943–3969.

Alexander C. M. O'D. and Wang J. 2001. Iron isotopes in chondrules: Implications for the role of evaporation during chondrule formation. *Meteoritics & Planetary Science* 36:419–428.

Amelin Y., Krot A. N., Hutcheon I. D., and Ulyanov A. A. 2002. Lead isotopic ages of chondrules and calcium-aluminum-rich inclusions. *Science* 297:1678–1683.

Amelin Y., Krot A. N., and Twelker E. 2004. Pb isotopic age of the CB chondrite Gujba, and the duration of the chondrule formation interval (abstract). *Geochimica et Cosmochimica Acta* 68:E958.

Beckett J. R., Simon S. B., and Stolper E. 2000 The partitioning of Na between melilite and liquid: Part II. Applications to type B inclusions from carbonaceous chondrites. *Geochimica et Cosmochimica Acta* 64:2519–2534.

Bizzarro M., Baker J. A., and Haack H. 2004. Mg isotope evidence for contemporaneous formation of chondrules and refractory inclusions. *Nature* 431:275–278.

Bonal L., Quirico E., Bourot-Denise M., and Montagnac G. 2006. Determination of the petrologic type of CV3 chondrites by Raman spectroscopy of included organic matter. *Geochimica et Cosmochimica Acta* 70:1849–1863.

Catanzaro E., Murphy T., Garner E., and Shields W. 1966. Absolute isotopic abundance ratios and atomic weight of magnesium. *Journal of Research of the National Bureau of Standards* 70A: 453.

Clayton R. N. 1993. Oxygen isotopes in meteorites. *Annual Review of Earth & Planetary Sciences* 21:115–149.

Cuzzi J. N. and Alexander C. M. O'D. 2006. Chondrule formation in particle-rich nebular regions at least hundreds of kilometres across. *Nature* 441:483–485.

Davis A. M. and MacPherson G. J. 1996. Thermal processing in the solar nebula: Constraints from refractory inclusions. In *Chondrules and the protoplanetary disk*, edited by Hewins R. H., Jones R. H., and Scott E. R. D. Cambridge: Cambridge University Press. pp. 71–77.

Davis A. M., Alexander C. M. O'D., Nagahara H., and Richter F. M. 2005. Evaporation and condensation during CAI and chondrule formation. In *Chondrites and the protoplanetary disk*, edited by Krot A. N., Scott E. R. D., and Reipurth B. ASP Conference Series #341. San Francisco: Astronomical Society of the Pacific. pp. 432–456.

Desch S. J. and Connolly H. C., Jr. 2002. A model of the thermal processing of particles in the solar nebula shocks: Application to the cooling rates of chondrules. *Meteoritics & Planetary Science* 37:183–207.

Fagan T. J., Krot A. N., Keil K., and Yurimoto H. 2003. Nebular setting of oxygen isotopic alteration in a coarse-grained Ca-Al-rich inclusion from Efremovka. *Meteoritics & Planetary Science* 39:1257–1272.

Fagan T. J., MacPherson G. J., and Kim G. L. 2004. Deciphering multiple alteration events in Allende Ca-Al-rich inclusions (abstract). *Meteoritics & Planetary Science* 39:A38.

Fagan T. J., Guan Y., and MacPherson G. J. 2006. Al-Mg isotopic constraints on alteration of Allende Ca-Al-rich inclusions (abstract #1213). 36th Lunar and Planetary Science Conference. CD-ROM.

Galy A., Young E. D., Ash R. D., and O'Nions R. K. 2000. The formation of chondrules at high gas pressures in the solar nebula. *Science* 290:1751–1753.

Gounelle M., Shu F. H., Shang H., Glassgold A. E., Rehm E. K., and Lee T. 2001. Extinct radioactivities and protosolar cosmic-rays: Self-shielding and light elements. *The Astrophysical Journal* 548: 1051–1070.

Gounelle M., Shu F. H., Shang H., Glassgold A. E., Rehm E. K., and Lee T. 2006. The irradiation origin of beryllium radioisotopes and other short-lived radionuclides. *The Astrophysical Journal* 640:1163–1170.

Greenwood J. P. 2004. Disequilibrium melting of refractory inclusions: A mechanism for high-temperature oxygen isotope exchange in the solar nebula (abstract #2132). 35th Lunar and Planetary Science Conference. CD-ROM.

Greenwood J. P. and Hess P. C. 1996. Congruent melting kinetics: Constraints on chondrule formation. In *Chondrules and the protoplanetary disk*, edited by Hewins R. H., Jones R. H., and Scott E. R. D. Cambridge: Cambridge University Press. pp. 205–213.

Grossman L. 1973. Petrography and mineral chemistry of Ca-rich inclusions in the Allende meteorite. *Geochimica et Cosmochimica Acta* 39:433–454.

Grossman L., Ebel D. S., and Simon S. B. 2002. Formation of refractory inclusions by evaporation of condensate precursors. *Geochimica et Cosmochimica Acta* 66:145–161.

Hsu W., Wasserburg G. J., and Huss G. R. 2000. High time resolution by use of the ^{26}Al chronometer in the multistage formation of a CAI. *Earth and Planetary Science Letters* 182:15–29.

Huss G. R., MacPherson G. J., Wasserburg G. J., Russell S. S., and Srinivasan G. 2001 Aluminum-26 in calcium-aluminum-rich inclusions and chondrules from unequilibrated ordinary chondrites. *Meteoritics & Planetary Science* 36:975–997.

Hutcheon I. D. and Newton R. C. 1981. Mg isotopes, mineralogy, and mode of formation of secondary phases in C3 refractory inclusions (abstract). 12th Lunar and Planetary Science Conference. pp. 491–493.

Itoh S. and Yurimoto H. 2003. Contemporaneous formation of chondrules and refractory inclusions in the early solar system. *Nature* 423:728–731.

Itoh S., Kojima H., and Yurimoto H. 2004. Petrography and oxygen isotopic compositions in refractory inclusions from CO chondrites. *Geochimica et Cosmochimica Acta* 68:183–194.

Ito M., Nagasawa H., and Yurimoto H. 2004. Oxygen isotopic SIMS analysis in Allende CAI: Details of the very early thermal history of the solar system. *Geochimica et Cosmochimica Acta* 68:2905–2923.

Jones R. H., Lee T., Connolly H. C., Jr., Love S. G., and Shang H. 2000. Formation of chondrules and CAIs: Theory versus observation. In *Protostars and planets IV*, edited by Mannings V., Boss A. P., and Russell S. S. Tucson, Arizona: The University of Arizona Press. pp. 927–962.

Kennedy A. K. and Hutcheon I. D. 1992. Chemical and isotopic constraints on the formation and crystallization of SA-1, a basaltic Allende plagioclase–olivine inclusion. *Meteoritics* 27: 539–559.

Kirkpatrick R. J. 1975. Crystal growth from the melt: A review. *American Mineralogist* 60:798–814.

Kita N. T., Nagahara H., Togashi S., and Morishita Y. 2000. A short duration of chondrule formation in the solar nebula: Evidence from ^{26}Al in Semarkona ferromagnesian chondrules. *Geochimica et Cosmochimica Acta* 64:3913–3922.

Kita N. T., Huss G. R., Tachibana S., Amelin Y., Nyquist L. E., and Hutcheon I. D. 2005. Constraints on the origin of chondrules and CAIs from short-lived and long-lived radionuclides. In *Chondrites and the protoplanetary disk*, edited by Krot A. N., Scott E. R. D., and Reipurth B. ASP Conference Series #341. San Francisco: Astronomical Society of the Pacific. pp. 558–588.

Krot A. N. and Keil K. 2002. Anorthite-rich chondrules in CR and CH carbonaceous chondrites: Genetic link between Ca, Al-rich inclusions and ferromagnesian chondrules. *Meteoritics & Planetary Science* 37:91–111.

Krot A. N. and Wasson J. T. 1995. Igneous rims on FeO-rich and FeO-poor chondrules in ordinary chondrites. *Geochimica et Cosmochimica Acta* 59:4951–4966.

Krot A. N., Scott E. R. D., and Zolensky M. E. 1995. Mineralogic and chemical variations among CV3 chondrites and their components: Nebular and asteroidal processing. *Meteoritics* 30: 748–775.

Krot A. N., Petaev M. I., Scott E. R. D., Choi B.-G., Zolensky M. E., and Keil K. 1998. Progressive alteration in CV3 chondrites: More evidence for asteroidal alteration. *Meteoritics & Planetary Science* 33:1065–1085.

Krot A. N., Weber D., Greshake A., Ulyanov A. A., McKeegan K. D., Hutcheon I. D., Sahijpal S., and Keil K. 1999. Relic Ca,Al-rich inclusions in chondrules from the carbonaceous chondrites Acfer 182 and Acfer 094 (abstract #1511). 30th Lunar and Planetary Science Conference. CD-ROM.

Krot A. N., Ulyanov A. A., Meibom A., and Keil K. 2001a. Forsterite-rich accretionary rims around Ca, Al-rich inclusions from the reduced CV3 chondrite Efremovka. *Meteoritics & Planetary Science* 36:611–628.

Krot A. N., Hutcheon I. D., and Huss G. R. 2001b. Aluminum-rich chondrules and associated refractory inclusions in the unique carbonaceous chondrite Adelaide (abstract). *Meteoritics & Planetary Science* 36:A105–A106.

Krot A. N., Meibom A., Weisberg M. K., and Keil K. 2002a. The CR chondrite clan: Implications for early solar system processes. *Meteoritics & Planetary Science* 37:1451–1490.

Krot A. N., McKeegan K. D., Leshin L. A., MacPherson G. J., and Scott E. R. D. 2002b. Existence of an ^{16}O-rich gaseous reservoir in the solar nebula. *Science* 295:1051–1054.

Krot A. N., Hutcheon I. D., and Keil K. 2002c. Anorthite-rich chondrules in the reduced CV chondrites: Evidence for complex formation history and genetic links between CAIs and ferromagnesian chondrules. *Meteoritics & Planetary Science* 37: 155–182.

Krot A. N., Fagan T. J., Yurimoto H., and Petaev M. I. 2004a. Amoeboid olivine aggregates with low-Ca pyroxenes: A genetic link between refractory inclusions and chondrules? *Geochimica et Cosmochimica Acta* 68:1929–1941.

Krot A. N., Fagan T. J., Yurimoto H., and Petaev M. I. 2004b. Origin of low-Ca pyroxene in amoeboid olivine aggregates: Evidence from oxygen isotopic compositions. *Geochimica et Cosmochimica Acta* 68:1873–1881.

Krot A. N., Fagan T. J., Keil K., McKeegan K. D., Sahijpal S., Hutcheon I. D., Petaev M. I., and Yurimoto H. 2004c. Ca,Al-rich inclusions, amoeboid olivine aggregates, and Al-rich chondrules from the unique carbonaceous chondrite Acfer 094: I. Mineralogy and petrology. *Geochimica et Cosmochimica Acta* 68:2167–2184.

Krot A. N., Petaev M. I., Russell S. S., Itoh S., Fagan T., Yurimoto H., Chizmadia L., Weisberg M. K., Komatsu M., Ulyanov A. A., and Keil K. 2004d. Amoeboid olivine aggregates in carbonaceous chondrites: Records of nebular and asteroidal processes. *Chemie der Erde* 64:185–239.

Krot A. N., Yurimoto H., Petaev M. I., Hutcheon I. D., and Wark D. A. 2004e. Type C CAIs: New insights into the early solar system processes (abstract). *Meteoritics & Planetary Science* 39: A57.

Krot A. N., Libourel G., Goodrich C. A., and Petaev M. I. 2004f. Silica-rich igneous rims around magnesian chondrules in CR carbonaceous chondrites: Evidence for fractional condensation during chondrule formation. *Meteoritics & Planetary Science* 39: 1931–1955.

Krot A. N., Hutcheon I. D., Yurimoto H., Cuzzi J. N., McKeegan K. D., Scott E. R. D., Libourel G., Chaussidon M., Aléon J., and Petaev M. I. 2005a. Evolution of oxygen isotopic composition in the inner solar nebula. *The Astrophysical Journal* 622:1333–1342.

Krot A. N., Yurimoto H., Hutcheon I. D., and MacPherson G. J. 2005b. Relative chronology of CAI and chondrule formation: Evidence from chondrule-bearing igneous CAIs. *Nature* 434: 998–1001.

Krot A. N., Yurimoto H., McKeegan K. D., Leshin L., Chaussidon M., Libourel G., Yoshitake M., Huss G. R., Guan Y., and Zanda B. 2006a. Oxygen isotopic compositions of chondrules: Implications for evolution of oxygen isotopic reservoirs in the inner solar nebula. *Chemie der Erde*, doi: 10.1016/j.chemer.2006.07.002.

Krot A. N., Hutcheon I. D., Brearley A. J., Pravdivtseva O. V., Petaev M. I., and Hohenberg C. M. 2006b. Time scales for secondary alteration of chondritic meteorites. In *Meteorites and the early solar system II*, edited by Lauretta D. and McSween H., Jr. Tucson, Arizona: The University of Arizona Press. pp. 525–555.

Krot A. N., Yurimoto H., Hutcheon I. D., Libourel G., Chaussidon M., Petaev M. I., MacPherson G. J., Paque-Heather J., and Wark D. A. 2007. Anorthite-rich, igneous (type C) Ca,Al-rich inclusions from the CV carbonaceous chondrite Allende: Evidence for multistage formation history. *Geochimica et Cosmochimica Acta* 71:4342–4364.

Kuo L. C. and Kirkpatrick R. J. 1985. Kinetics of crystal dissolution in the system forsterite-diopside-silica. *American Journal of Science* 285:51–90.

LaTourrette T. and Wasserburg G. J. 1998. Mg diffusion in anorthite: Implications for the formation of early solar system planetesimals. *Earth and Planetary Science Letters* 158:91–108.

Libourel G., Krot A. N., Tissandier L., and Robert F. 2002. Open system behavior of common and moderately volatile elements during chondrule formation (abstract). *Meteoritics & Planetary Science* 37:A87.

MacDougall J. D., Kerridge J. F., and Phinney D. 1981. Refractory ABC (abstract). 12th Lunar and Planetary Science Conference. pp. 643–645.

MacPherson G. J. 2003. Calcium-aluminum-rich inclusions in chondritic meteorites. In *Meteorites, comets, and planets*, edited by Davis A. M. Treatise on Geochemistry, vol. 1. Oxford: Elsevier-Pergamon. pp. 201–246.

MacPherson G. J. and Davis A. M. 1993. A petrologic and ion microprobe study of a Vigarano type B2 refractory inclusion: Evolution by multiple stages of alteration and melting. *Geochimica et Cosmochimica Acta* 57:231–243.

MacPherson G. J., Davis A. M., and Zinner E. K. 1995. The distribution of aluminum-26 in the early solar system. *Meteoritics* 30:365–386.

Maruyama S. and Yurimoto H. 2003. Relationships among O, Mg isotopes, and the petrography of two spinel-bearing chondrules. *Geochimica et Cosmochimica Acta* 67:3943–3957.

Maruyama S., Yurimoto H., and Sueno S. 1999. Oxygen isotope evidence regarding the formation of spinel-bearing chondrules. *Earth and Planetary Science Letters* 169:165–171.

McGuire A. V. and Hashimoto A. 1989. Origin of zoned fine-grained inclusions in the Allende meteorite. *Geochimica et Cosmochimica Acta* 53:1123–1133.

Misawa K. and Nakamura N. 1988. A relict refractory inclusion in a ferromagnesian chondrule from the Allende meteorite. *Nature* 334:723–726.

Mostefaoui S., Kita N. T., Togashi S., Tachibana S., Nagahara H., and Morishita Y. 2002. The relative formation ages of ferromagnesian chondrules inferred from their initial aluminum-26/aluminum-27 ratios. *Meteoritics & Planetary Science* 37:421–438.

Nagashima K., Yoshitake M., and Yurimoto H. 2004. Oxygen isotope exchange recorded within anorthite single crystal in Vigarano CAI: Evidence for remelting by high-temperature process in the solar nebula (abstract #9072). Workshop on Chondrites and the Protoplanetary Disk. CD-ROM.

Nomura K. and Miyamoto M. 1998. Hydrothermal experiments on alteration of Ca-Al-rich inclusions CAIs in carbonaceous chondrites: Implication for aqueous alteration in parent asteroids. *Geochimica et Cosmochimica Acta* 62:3575–3588.

Paque J. M., Beckett J. R., Barber D. J., and Stolper E. M. 1994. A new titanium-bearing caclium aluminosilicate phase: I. Meteoritic occurrences and formation in synthetic systems. *Meteoritics* 29:673–682.

Richter F. M., Davis A. M., Ebel D. S., and Hashimoto A. 2002. Elemental and isotopic fractionation of type B calcium-, aluminum-rich inclusions: Experiments, theoretical considerations, and constraints on their thermal evolution. *Geochimica et Cosmochimica Acta* 66:521–540.

Russell S. S., Srinivasan G., Huss G. R., Wasserburg G. J., and MacPherson G. J. 1996. Evidence for widespread ^{26}Al in the solar nebula and constraints for nebula time scales. *Science* 273:757–762.

Russell S. S., Krot A. N., MacPherson G. J., Huss G. R., Itoh S., Yurimoto H., and Keil K. 2005. Genetic relationship between refractory inclusions and chondrules. In *Chondrules and the protoplanetary disk*, edited by Krot A. N., Scott E. R. D., and Reipurth B. ASP Conference Series #341. San Francisco: Astronomical Society of the Pacific. pp. 317–353.

Ryerson F. J. and McKeegan K. D. 1994. Determination of oxygen self-diffusion in åkermanite, anorthite, diopside, and spinel: Implications for oxygen isotopic anomalies and the thermal histories of Ca-Al-rich inclusions. *Geochimica et Cosmochimica Acta* 58:3713–3734.

Scott E. R. D. and Krot A. N. 2003. Chondrites and their components. In *Meteorites, comets and planets*, edited by Davis A. M. Treatise on Geochemistry, vol. 1. Oxford: Elsevier-Pergamon. pp. 143–200.

Stolper E. 1986. Crystallization sequences of Ca-Al-rich inclusions from Allende: An experimental study. *Geochimica et Cosmochimica Acta* 46:2159–2180.

Thrane K., Bizzarro M., and Baker J. A. 2006. Extremely brief formation interval for refractory inclusions and uniform ^{26}Al in the early solar system. *The Astrophysical Journal* 646:L159–L162.

Tissandier L., Libourel G., and Robert F. 2002. Gas-melt interactions and their bearings on chondrule formation. *Meteoritics & Planetary Science* 37:1377–1389.

Wark D. A. 1987. Plagioclase-rich inclusions in carbonaceous chondrite meteorites: Liquid condensates? *Geochimica et Cosmochimica Acta* 51:221–242.

Wark D. A. and Boynton W. V. 2001. The formation of rims on calcium-aluminum-rich inclusions: Step I—Flash heating. *Meteoritics & Planetary Science* 36:1135–1166.

Wark D. A. and Lovering J. F. 1977. Marker events in the early solar system: Evidence from rims on Ca-Al-rich inclusions in carbonaceous chondrites. Proceedings, Eighth Lunar Science Conference. pp. 95–112.

Wasson J. T., Yurimoto H., and Russell S. S. 2001. ^{16}O-rich melilite in CO3 chondrites; The possible formation of common ^{16}O-poor melilite by aqueous alteration. *Geochimica et Cosmochimica Acta* 65:4539–4549.

Yurimoto H., Ito M., and Nagasawa H. 1998. Oxygen isotope exchange between refractory inclusion in Allende and solar nebula gas. *Science* 282:1874–1877.

Yurimoto H. and Kuramoto K. 2004. Molecular cloud origin for the oxygen isotope heterogeneity in the solar system. *Science* 305: 1763–1766.

Yurimoto H., Koike O., Nagahara H., Morioka M., and Nagasawa H. 2000. Heterogeneous distribution of Mg isotopes in anorthite single crystal from type B CAIs in Allende meteorite (abstract #1593). 31st Lunar and Planetary Science Conference. CD-ROM.